

LIQUID METAL EMBRITTLEMENT OF
TYPE 304 STAINLESS STEEL
BY LIQUID MERCURY

By

TIMOTHY JOHN CLARK

Bachelor of Science

Oklahoma State University

Stillwater, Oklahoma

1993

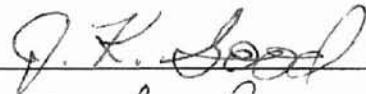
Submitted to the Faculty of the
Graduate College of the
Oklahoma State University
in partial fulfillment of
the requirements for
the Degree of
MASTER OF SCIENCE
December, 1995

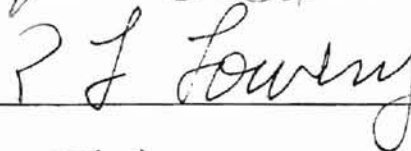
LIQUID METAL EMBRITTLEMENT OF
TYPE 304 STAINLESS STEEL
BY LIQUID MERCURY

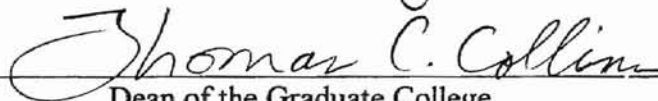
Thesis Approved:



Thesis Adviser







Dean of the Graduate College

ACKNOWLEDGMENTS

I would like to thank my major adviser, Dr. C. E. Price, for his guidance, shared knowledge, and inspiration throughout this project, as well as through several graduate and undergraduate courses. Moreover, I thank Dr. Price and the department of Mechanical and Aerospace Engineering for financial support facilitating my graduate study. Also, I thank my additional committee members, Dr. J. K. Good and Dr. R. L. Lowery, without whom completion of this project would not have been possible.

Additionally, I thank my parents, Richard and Linda Clark, for their support, both emotional and financial, through these years of study.

Finally, I thank all my friends, particularly those in the house movement, for their undying support, encouragement, and love, without which projects of this magnitude would certainly never see fruition.

TABLE OF CONTENTS

Chapter	Page
1. INTRODUCTION.....	1
2. BACKGROUND.....	1
Selectivity of Embrittlement.....	2
Embrittlement Mechanisms.....	3
Requirements for Embrittlement.....	5
Variables Affecting Embrittlement.....	7
Fatigue Behavior in Liquid Metal Environments.....	14
Comparison With Other Forms of Embrittlement.....	15
Liquid Metal Induced Embrittlement of Nickel, Nickel-Based Alloys, and Austenitic Stainless Steels.....	16
Liquid Metal Embrittlement of Nickel and Nickel-Based Alloys in Slow Strain Rate Testing.....	16
Liquid Metal Embrittlement of Nickel and Nickel-Based Alloys in Fatigue Testing.....	29
Liquid Metal Embrittlement of Type 304 Stainless Steel.....	37
Discussion.....	37
3. PROPOSED STUDY.....	42
4. EXPERIMENTAL PROCEDURE.....	44
Material.....	44
Heat Treatment.....	44
Polishing and Etching.....	45
Grain Size Determination.....	47
Specimen Preparation.....	47
Testing.....	50
Microscopy.....	52
Wetting.....	52
5. RESULTS.....	54
Initial Results.....	54

5. RESULTS.....	54
Initial Results.....	54
Strain Rate.....	64
Sensitization.....	66
Grain Size.....	69
Prior Cold Work.....	71
Fatigue.....	71
6. DISCUSSION.....	77
Wetting Behavior.....	77
Comparison With Nickel Base Alloy Embrittlement Behavior.....	77
Similarity to 800 Series Nickel Base Alloy Behavior.....	79
Similarity to Alloy 600 With Respect to Sensitization.....	79
Nucleation Versus Propagation Control.....	80
7. SUMMARY OF RESULTS.....	81
8. SUGGESTIONS FOR FURTHER RESEARCH.....	82
BIBLIOGRAPHY.....	84

LIST OF TABLES

Table		Page
I.	Chemical Composition of N80000 and S30400.....	43
II.	Baseline Data.....	54
III.	Embrittlement vs. Grain Size.....	64
IV.	Embrittlement vs. Sensitization.....	66
V.	Embrittlement vs. Grain Size.....	69
VI.	Embrittlement vs. Prior Cold Work.....	71
VII.	Embrittlement vs. Fatigue.....	71

LIST OF FIGURES

Figure		Page
1.	Schematic illustrating reduction of strength of atomic bond at crack tip by embrittler species	3
2.	Schematic illustrating crack growth by microvoid coalescence and the reduction in shear strength of atomic bonds by embrittler species atoms.....	5
3.	Variation of flow stress and fracture stress with grain size of zinc in liquid mercury.....	9
4.	Typical embrittlement vs. temperature diagram.....	10
5.	(a) The cup of ductile SSR failure of Nickel 200 in air. (b) Nickel 200 failure in mercury, slant fracture with several origins, especially at lower edge.....	18
6.	(a) Close-up of necked region of Nickel 200; note intense slip, slant cracking. (b) Origin zone of Nickel 200 fracture; irregular contours, tearing, slip traces evident. (c) Some origin zones on Nickel 200 were more transgranular. Secondary slip traces show clearly. (d) Nickel 200 transition from transgranular to MVC.....	19
7.	Alloy 400 fractured in mercury. (a) Totally intergranular nature of break. (b) Close-up of intergranular break, typical throughout cross section.....	20
8.	Reduction of area versus temperature, Alloy 400 fractured in mercury.....	21
9.	Alloy R405. (a) Note presence of some necking, no cup and cone, however. (b) In midsection, slip markings, tearing, possible dimple rupture, as opposed to transgranular edge zone. (c) Side view showing extensive surface cracking.....	23
10.	Typical fracture surface, Alloy K500. Similar to Alloy 400; note surface irregularities.....	24

11.	Alloy 718 fracture surface. (a) Mixed mode macroscopic fracture appearance. Mainly flat, with slant zone at top, as viewed. (b) Intergranular origin zone; note second-phase pock-marks. (c) Curious combination of dimple rupture and intergranular separation at transition to slant region.....	26
12.	Fracture surface, Alloy X750. (a) Intergranular origin zone with relatively large amount of tearing. (b) Conglomeration of various effects in later stages of fracture.....	27
13.	Alloy 800 fracture. (a) Cup and cone fracture. (b) Detail of (a) showing dimpled rupture failure mode. No embrittlement evident; Alloy 825 same.....	28
14.	Fracture surface of Nickel 200 fatigued in mercury. (a) Origin zone; note clean grain boundaries, lack of secondary grain boundary cracking, and that some grains are sheared across. (b) Transition region between IG and TG, secondary cracking present. (c) Transition between TG and MVC abrupt overload failure.....	30
15.	Opened out secondary crack in cold worked Alloy 400; note clean, elongated grains and intergranular cracking in the third orthogonal direction.....	32
16.	Alloy 600 fracture surface. (a) Predominately intergranular origin zone. (b) Detail of origin zone; note shear failures in minority of grains and occasional secondary cracking. (c) Detail of origin zone; note second phase particles and transgranular fracture of one grain. (d) Later stage of failure, primarily TG, but with some secondary IG cracking.....	33
17.	Alloy 718 fatigue fracture in mercury. (a) Transgranular cracking with traces of intergranular cracking. (b) Detail of (a) showing individual grain; note slip, or possible striation, markings on surrounding grains. (c) Intermediate stage of failure; note extensive secondary cracking of IG and TG nature. (d) Late stage of failure; note well defined striations and minimal secondary cracking.....	35
18.	Fracture surfaces of (a) Alloy 800 and (b) Alloy 825. (a) Fatigue origin zone, primarily IG. (b) Fatigue origin zone, mixed mode cracking and slip, or possibly striations.....	36
19.	Typical Type 304 test specimen.....	38

20.	Fracture surface of Type 304 tested at varying strain rates. (a) $5 \times 10^{-7} \text{ s}^{-1}$. (b) $1 \times 10^{-4} \text{ s}^{-1}$. (c) $3.3 \times 10^{-3} \text{ s}^{-1}$. (d) $8.3 \times 10^{-3} \text{ s}^{-1}$	39
21.	Fracture surface of Type 304 tested in mercury at $5 \times 10^{-6} \text{ s}^{-1}$. (a) Embrittled outer region. (b) Ductile central region.....	40
22.	Grain growth vs. time. (a) Reference chart. (b) Experimental results.....	46
23.	Typical microstructural appearance of (a) unsensitized (Step Structure) and (b) sensitized (Ditch Structure) stainless steel.....	48
24.	Specimen dimensions (actual total length 6 in.).....	49
25.	Apparatus for testing in mercury.....	51
26.	Unwetting drops of mercury on (a) 600-grit polished surface (SZM) and (b) fracture surface (SEM, $100\times$).....	53
27.	As-received specimen broken in air. (a) General specimen view, $20\times$. (b) Detail, showing microvoids as well as secondary MVC cracking, $1000\times$	55
28.	As-received specimen broken in mercury. (a) General specimen view, $20\times$. Note MVC smooth region, lower left. (b) Detail, $1000\times$. Note cleaved slip bands as well as some prominent slip bands on the sheared grain at the upper right.....	58
29.	Annealed specimen broken in mercury. (a) General view, $20\times$. (b) Detail, $100\times$. (c) Detail, showing TG + IG mixed-mode cracking, $500\times$. This particular zone has an unusually high amount of IG contribution. (d) Detail of (c), $1500\times$. IG region; note slip on three systems, secondary cracking. (e) Detail of TG region of Figure 29 (c), $1500\times$. (f) Side view of fracture surface/specimen side interface, $60\times$. (g) Side view of fracture surface, $300\times$. (h) Side of specimen near fracture, $300\times$. (i) Side, 6-8 mm from fracture, $300\times$. (j) Side, between Figure 29 (h) and (i), $1000\times$..	59
30.	Fracture surfaces at various strain rates. (a) $5 \times 10^{-7} \text{ s}^{-1}$. (b) $1 \times 10^{-4} \text{ s}^{-1}$. (c) $3.3 \times 10^{-3} \text{ s}^{-1}$. (d) $8.3 \times 10^{-3} \text{ s}^{-1}$	65
31.	Fracture surface of sensitized specimen broken in mercury. (a) General specimen view, $20\times$. (b) Detail, $200\times$	67

32. Sensitized small-grained specimen broken in mercury, 20×. Note MVC region at lower left. The origin is likely at upper right; note secondary cracking is much more conspicuous as the crack progresses.....68
33. (a) 250–400 μm grain size specimen, broken in mercury, 20×. Note TG region at lower portion of fracture. (b) 25–35 μm grain size specimen, broken in mercury, 20×. Isolated small TG patches were found at 9 and 12 o'clock.....70
34. Fracture surface of annealed and cold-worked (to 70% of the tensile strength) specimen. (a) General view, 20×. (b) Detail, from 12 o'clock, showing TG origin zone and transition to MVC, 500×...72
35. Annealed specimen broken in fatigue in liquid mercury. (a) General specimen view, 20×. (b) Mixed-mode origin, 1000×. (c) More advanced stage of fatigue crack, 500×. Note larger TG contribution. (d) Later stage of crack, 500×. Note more plastic deformation, TG cleavage, yet some IG. Note possible remains of striations, as indicated by arrow. (e) End of fatigue crack, 500×. Note large extent of PD and secondary cracking.....74

NOMENCLATURE

d	grain diameter
FCC	face centered cubic
GS	grain size
HE	hydrogen embrittlement
HRB	hardness, Rockwell B
HRC	hardness, Rockwell C
IG	intergranular
LMIE	liquid metal induced embrittlement
MIE	metal induced embrittlement
MVC	microvoid coalescence
PD	plastic deformation
RA	reduction of area
SCC	stress corrosion cracking
SEM	scanning electron microscope
SFE	stacking fault energy
SMIE	solid metal induced embrittlement
SSR	slow strain rate
SZM	stereoscopic zoom microscope
TG	transgranular

CHAPTER 1

INTRODUCTION

Liquid metal induced embrittlement (LMIE) refers to the presence of a liquid metal environment lowering a normally ductile metal's fracture toughness or ductility at fracture [1]. In the last ten years at Oklahoma State University, LMIE of nickel-base alloys by liquid mercury has been extensively investigated. Additionally, it is known that austenitic stainless steel and liquid mercury constitute an embrittlement couple. Due to compositional and structural similarities between nickel-base alloys and austenitic stainless steels, it can be inferred that some similarity of embrittlement behavior in liquid mercury environments should exist. Therefore, the thrust of the present study is to first summarize embrittlement behaviors and phenomena in the nickel-base alloys resulting from earlier studies. Then, AISI Type S30400, the most widely used commercial austenitic stainless steel, will be examined to determine if the same generalizations for embrittlement phenomena in nickel-base alloys hold for embrittlement of austenitic stainless steels.

CHAPTER 2

BACKGROUND

Liquid metal induced embrittlement (LMIE) is the loss of ductility or fracture toughness of a normally ductile metal when stressed in the presence of a liquid metal environment. LMIE occurrences in service can be disastrous, as affected metals often fail catastrophically, with little or no warning, and at stresses below their normal tensile strength [1,2]. Crack velocities up to 5 ms^{-1} have been reported [3]. LMIE generally results in a decrease in reduction of area and per cent elongation at failure; true fracture stress is correspondingly reduced and may be below the macroscopic yield strength in instances of severe embrittlement. Flow behavior remains unchanged in embrittling liquid environments, however; therefore yield strength, Young's modulus, and work-hardening behavior are unaffected. The stress-strain curve is unchanged by LMIE occurring, up to the point of failure. LMIE has been known to occur since 1874, but, due to its relatively uncommon nature, it has not been investigated to the extent that hydrogen embrittlement, temper embrittlement, and stress corrosion cracking have been studied [1].

SELECTIVITY OF EMBRITTLEMENT

LMIE occurs in specific pairs of metals; for example, aluminum/liquid gallium is an embrittlement couple but magnesium/liquid gallium is not. Additionally, certain metals are known to be embrittled by solid metals (SMIE). LMIE thus falls into the more general category of metal induced embrittlement (MIE) [4]. For example, solid cadmium embrittles titanium and steels. Embrittlement can also occur where an embrittling metal exists as an inclusion or second phase in the embrittled metal. This phenomenon can occur both with liquid- and solid metal induced embrittlement, e.g., hot-shortness of copper-containing steels and lead embrittlement of internally leaded steels, respectively

[1,2]. From equilibrium phase diagrams of most known LMIE couples, two empirical rules have been developed concerning whether a pair of metals will constitute an embrittlement couple. First, if the metals form stable high melting point intermetallic compounds in the solid state, an embrittlement couple is unlikely to result. Second, high mutual solubility between two metals also generally precludes the constitution of an embrittlement couple [1]. Some exceptions to these rules exist, but they generally hold. The correlation between intermetallic compound formation and resistance to embrittlement is not well understood. However, high mutual solubility can limit embrittlement by allowing dissolution of the solid metal at the crack tip, causing crack tip blunting (the Joffe effect) [2,5]. Also, embrittlement may not occur in a likely couple if the solid metal is highly ductile near the melting temperature of the liquid metal. Such a material may be ductile enough to completely prevent formation or propagation of a brittle crack, regardless of the presence of the liquid metal [2].

EMBRITTLEMENT MECHANISMS

Two principal mechanisms are widely accepted for liquid metal embrittlement [6]. The first is that adsorption of liquid metal atoms induces a localized reduction in the cohesive strength of atomic bonds in the solid metal. When this event occurs at a stress concentration on the solid metal's surface, a crack is initiated; the process continues by the weakening of atomic bonds at the crack tip, facilitating crack propagation. Figure 1 shows this phenomenon. Under applied load F , embrittler atom B can be seen weakening the bond between solid metal atoms A and A_0 at the crack tip. The second mechanism involves a reduction in shear strength of atomic bonds by the adsorption of embrittler metal atoms. This localized reduction in shear strength facilitates nucleation of dislocations or slip at low stresses at or near the crack tip. The resulting localized increase

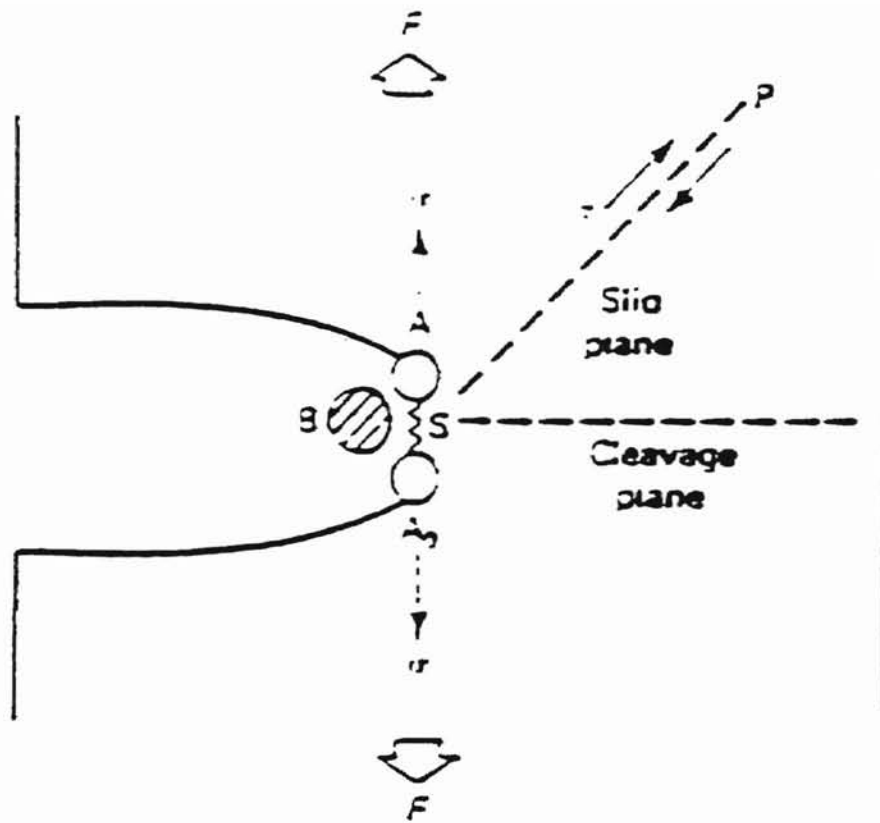
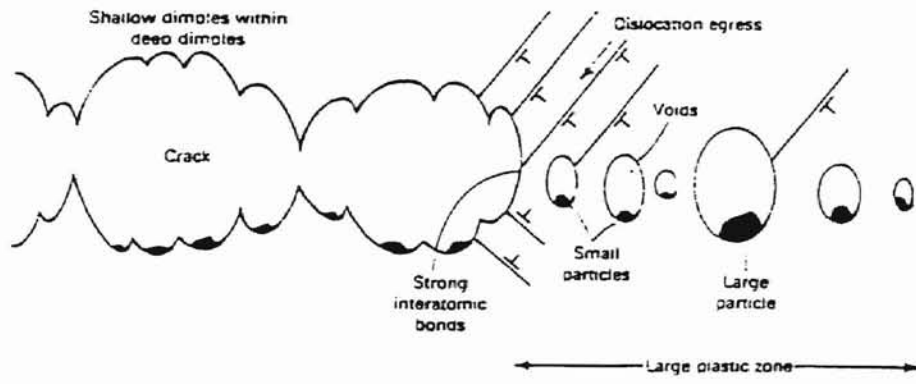


Figure 1. Schematic illustrating reduction of strength of atomic bond at crack tip by embrittler species [6].

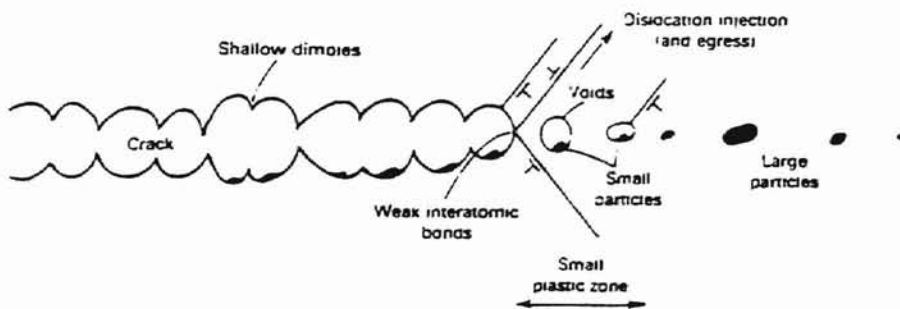
in plasticity facilitates the nucleation of voids ahead of the crack tip; as these voids grow, crack growth occurs. Figure 2 shows this process. Note the presence of weakened atomic bonds in the liquid metal environment. While this is actually a ductile process, macroscopically the material still suffers a loss of ductility, and is embrittled. Typically, LMIE results in a brittle intergranular or cleavage fracture mode due to the localized reduction in cohesion of atomic bonds. However, ductile dimpled fracture, caused by reduction in bond shear strength and resulting void nucleation, results in a transgranular failure mode [6]. Similar mechanisms are believed to be responsible for various forms of embrittlement, i.e., HE, MIE, etc.

REQUIREMENTS FOR EMBRITTLEMENT

For liquid metal embrittlement to occur, two basic requirements must be fulfilled. First, the solid metal must be wetted by the liquid metal. Failure to meet this criterion has led to the erroneous conclusion of immunity to LMIE for certain solid-liquid metal couples by some researchers [1]. For example, aluminum is embrittled by mercury, but liquid mercury will not wet an aluminum oxide film. Therefore, for aluminum to be embrittled in mercury, the oxide film must be defeated in some fashion [3]. Additionally, the liquid metal must be present at the crack tip for LMIE to continue in propagation-controlled embrittlement [6]. (In nucleation-controlled embrittlement, once a crack is initiated, it propagates to failure whether or not the embrittling metal is present at the crack tip. This type of embrittlement may occur, for example, in some martensitic steels [6].) There is some contention as to how liquid metal keeps up with a crack tip moving at velocities encountered in LMIE, considering that the crack tip is atomically sharp. The fact that embrittlement can occur near the melting temperature of the embrittling metal and that susceptibility to embrittlement is relatively independent of temperature may



(a)



(b)

Figure 2. Schematic illustrating crack growth by microvoid coalescence and the reduction in shear strength of atomic bonds by embrittler species atoms [6].

discount the possibility of diffusion of the liquid metal to the crack tip as a likely transport mechanism [2,6]. It has been suggested that a driving pressure of 10^5 atm would be required for bulk liquid metal to be present at an atomically sharp crack tip. Capillary effects are capable of providing negative pressures of 10^4 to 10^5 atm, which would effectively pull the liquid metal into contact with the crack tip [2]. Alternatively, diffusion processes may indeed be responsible for delivery of liquid metal atoms to the crack tip. Since the liquid metal atoms are known to be expendable in the embrittlement process, transport to the crack tip may occur by diffusion of a monolayer of liquid metal atoms over liquid metal atoms adsorbed onto the solid metal crack surface. Such second monolayer diffusion should be capable of maintaining a sufficient supply of liquid metal atoms at the crack tip to explain observed crack propagation rates [2]. The second requirement is that there is some degree of plastic deformation. Local plastic flow sufficient to cause LMIE cracking can be facilitated by stress concentrations at grain boundaries, second phase particles, and notches, so macroscopic plastic deformation is not required [1].

VARIABLES AFFECTING EMBRITTLEMENT

Several variables affect the occurrence and severity of LMIE. These variables include grain size, temperature, purity/composition, degree of cold work, and strain rate. Additionally, variables of the liquid itself affect the embrittlement process [2]. Grain size influences embrittlement because grain boundaries are obstacles to plastic flow, and therefore potential sites of stress concentration. Once plastic flow is blocked, dislocations pile up behind the obstacle, creating a local stress concentration. Larger grains facilitate larger pileups, and hence larger stress concentrations. However, if the grain size is too large, ready plastic deformation of the material may limit embrittlement. Within this limit, if it exists for a particular material, a larger grain size will facilitate a lower applied stress

to generate a high enough stress concentration for brittle fracture to occur [5]. Certain materials consequently exhibit a transition between nucleation- and propagation-controlled embrittlement as grain size decreases. Figure 3 shows this behavior in the zinc/mercury embrittlement couple. Note the linear relationship between fracture stress, σ_F , and grain diameter. Larger grain sizes in region I promote nucleation control, while smaller grain sizes of region II encourage propagation control. When tested in air, many ductile metals, e.g., copper, α brass, cadmium, and nickel, show the same fracture characteristics regardless of grain size. Sometimes, in appropriate liquid metal environments, σ_F is proportional to $d^{-1/2}$, and larger grain sizes require lower stresses to fracture [2].

In most cases, there is some degree of embrittlement susceptibility variation with temperature. Generally, embrittlement is maximum at the melting point of the environment. At sufficiently high temperatures, many couples exhibit a brittle-to-ductile transition where the solid metal is no longer susceptible to embrittlement. Such temperatures are not sharply defined and do not correlate theoretically with diffusion, dissolution, or other temperature-controlled processes. Similarly, many materials are not embrittled below a certain temperature. This variation of embrittlement, or lack thereof, with temperature gives rise to an embrittlement trough. This trough of embrittlement susceptibility may be from a few degrees to several hundred degrees Celsius wide. Figure 4 shows a typical embrittlement trough [5]. At low temperatures, limited wettability of the liquid metal is probably a limiting factor to embrittlement [7]. It is generally accepted that at high enough temperatures a material's tendency to behave in a ductile fashion may override any embrittling tendencies of the environment. For example, in smooth steel specimens tested in liquid lead, the brittle-ductile transition occurs at approximately 510 °C (950 °F), some 335 °C (600 °F) above the melting point of lead. The transition temperature also depends on strain rate and grain size; an increase in strain rate or decrease in grain size will raise the transition temperature [6]. SMIE is also influenced by temperature. SMIE generally does not occur below 75 % of the melting temperature of

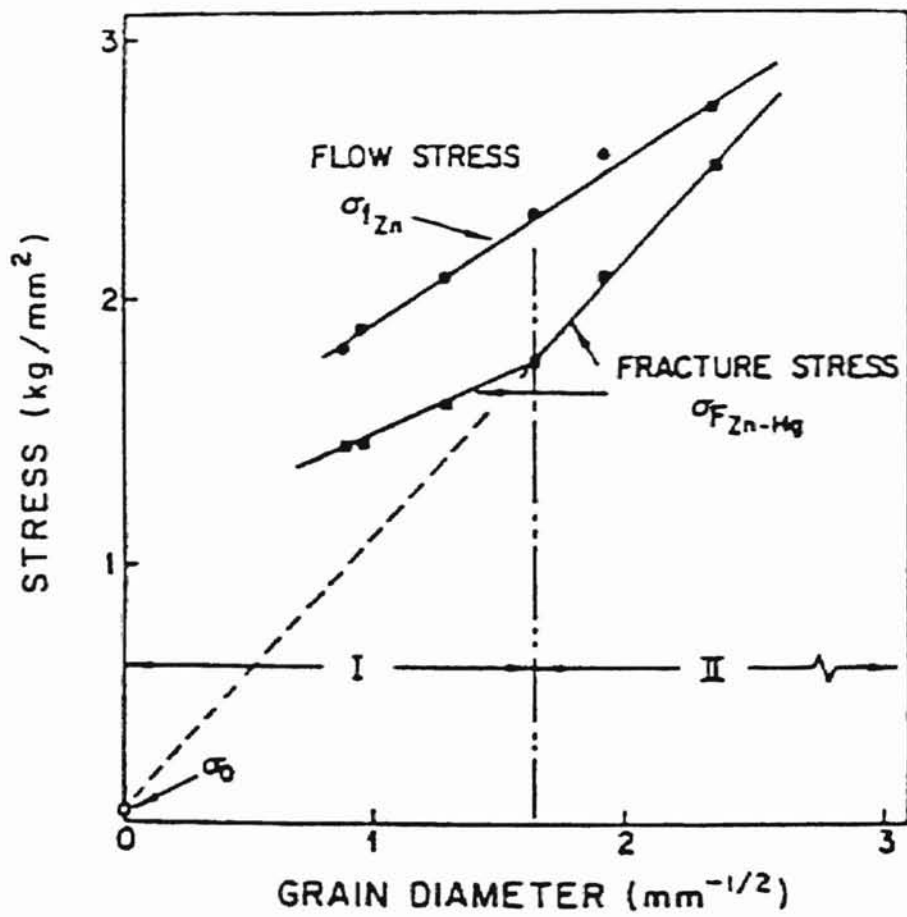


Figure 3. Variation of flow stress and fracture stress with grain size of zinc in liquid mercury [2].

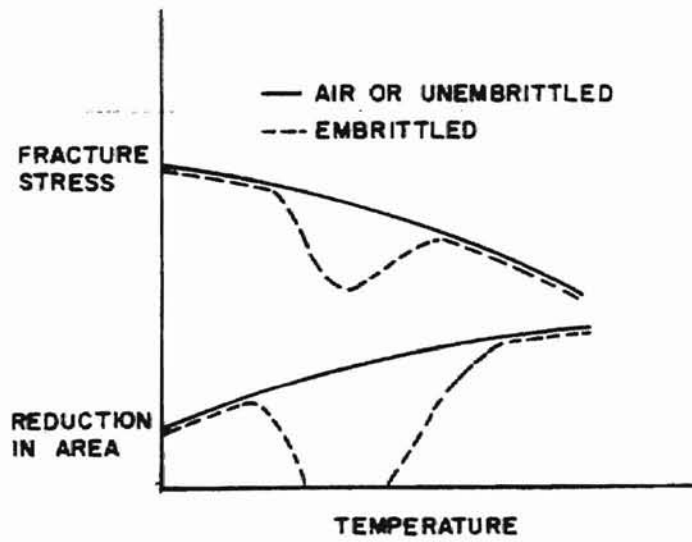


Figure 4. Typical embrittlement vs. temperature diagram [5].

the embrittling species, and solid metals that embrittle generally also embrittle in the liquid phase [5]. Additionally, some solid metals that fail to be embrittled by a potentially embrittling liquid metal, due to high ductility or mutual solubility at the liquid metal's melting point, may still be embrittled by that metal. This phenomenon can occur if the embrittling metal is dissolved in an inert carrier liquid metal. The embrittling species then exists effectively as a liquid at a temperature far below its own melting temperature. For example, indium does not easily embrittle cadmium because of cadmium's high ductility at indium's melting point, 156 °C (313 °F). However, mercury, which does not embrittle cadmium, dissolves up to 70 % indium at room temperature, and the indium in this solution severely embrittles cadmium [6]. It is interesting to note that the concept of inert carriers may be misunderstood, however. For example, in the above case, mercury may not embrittle cadmium due to lack of wetting; if the addition of indium to mercury were to facilitate wetting, then the mercury would be responsible for the embrittlement, and not simply an inert carrier. For example, AISI 4145 steel is not embrittled by liquid lead at 427 °C, but tin and antimony additions to the lead facilitate embrittlement, since Pb-Sn and Pb-Sb alloys are embrittling to steels at 427 °C. However, liquid lead alone embrittles 4145 at lower temperatures, and tin and antimony additions to the lead merely shift the ductility recovery temperature upwards in a continuous manner. The bottom line is that more than one variable may be involved when the idea of an inert carrier is proposed [5].

The composition of the solid metal also affects susceptibility to and degree of embrittlement. Generally, susceptibility of a pure metal to embrittlement is less than susceptibility of the same metal with solute additions. Furthermore, the susceptibility increases with increasing solute content. Iron- and copper-based alloys behave in this fashion. An increase in yield stress due to solid-solution hardening is considered responsible for this increase in embrittlement susceptibility. The yield stress increases with solute additions to the matrix, while stacking fault energy (SFE) decreases with increased solute concentrations. Low SFE means that dislocations piled up behind an obstacle, e.g.,

a grain boundary, cannot readily cross-slip; hence stress concentrations can quickly build with strain to levels sufficient to nucleate cracks. Alloying elements do not affect embrittlement susceptibility by altering the yield strength alone, however. Alloying can also affect the bond strength of an alloy, and hence the strength of bonds at a crack tip [2]. Nonmetallic impurities can also affect LMIE. For example, in copper-nickel alloys, phosphorus grain boundary precipitates reduce susceptibility to embrittlement by mercury; susceptibility and severity of embrittlement decreases with increasing phosphorus content. The amount of phosphorus required (on the order of $< .5\%$ P) to prevent embrittlement depends on the nickel content as well as on other alloying elements [8].

The amount of cold work or prestrain present in a metal will likely affect the degree of embrittlement, but there is material variation of what that effect will be. In non-age hardenable aluminum alloys tested in liquid mercury, susceptibility to embrittlement is decreased with increased cold work. In age hardenable aluminum alloys, cold work first increases susceptibility to embrittlement, then decreases susceptibility with higher amounts of prestrain, although it should be noted that such alloys can only undergo limited cold work. Embrittlement of α brass by mercury-sodium amalgam is severe with prestrains up to 25 % reduction of area; failure mode is intergranular. As the amount of cold work increases, embrittlement susceptibility decreases and failure mode becomes ductile and transgranular. The elimination of grain boundaries due to cold work may be the dominant factor responsible for this reduction in susceptibility and change in fracture mode [2]. Alloy 400 in liquid mercury becomes less embrittled with greater amounts of prestrain [9]. While not entirely predictable, the general trend is toward improved embrittlement resistance with increased amounts of cold work. This effect is somewhat intuitive, in that an intergranular fracture path is more difficult to achieve if the grains are elongated perpendicular to the direction of crack propagation. In internally leaded 4145 steel, embrittlement is eliminated by 50 % cold work. This effect is apparently due to the change in crack path from prior austenitic grain boundaries in undeformed samples to a

transgranular path along iron-iron carbide boundaries after deformation [5]. This author surmises a similar mechanism is likely at work in many instances of cold work-induced reduction of embrittlement susceptibility. Additionally, cold work increases energy throughout the material, and the energy gradient at grain boundaries is therefore lessened. Since LMIE is a localized effect attacking high energy sites, i.e. grain boundaries, this reduction in energy gradient at the grain boundaries corresponds to a lessening of embrittlement behavior.

Strain rate has an effect on embrittlement susceptibility in many systems. Embrittlement is generally more likely to occur, and is typically more severe, with slower strain rates. Alloy 400 illustrates this behavior in liquid mercury by showing a decrease in reduction in area from ~60 % at a strain rate of 10^{-2} s^{-1} to ~10 % at 10^{-6} s^{-1} [10].

Variables of the liquid metal itself are also important to the embrittlement process. Embrittlement is often slightly more severe close to the freezing temperature of the liquid metal. Presumably, this is due to temperature effects in the solid metal; i.e., ductility of the solid increases with temperature, hence embrittlement susceptibility drops. Also, substantial variations in the degree of embrittlement can be induced by small changes in the chemical composition of the liquid metal. For instance, Al-2024T3 in mercury is less susceptible to embrittlement if small amounts (up to 0.84 atomic %) of tin are dissolved in the mercury, while additions of ~3 at. % zinc or gallium to the mercury increase embrittlement markedly. It is likely that these changes in embrittlement are due to changes in wettability of the solid by the liquid; i.e., in this case tin apparently inhibits wetting, while zinc and gallium promote it [2]. 9Cr steel's susceptibility to embrittlement in liquid sodium can be greatly reduced or outright eliminated by removing oxygen and hydrogen impurities from the sodium [4]. Since aluminum oxide is not wetted by mercury, dissolved oxygen in mercury can inhibit embrittlement by promoting oxidation at the crack tip [3]. Additionally, wetting of aluminum by mercury may be facilitated by the presence of wetting agents, such as copper and zinc, in the mercury [11].

FATIGUE BEHAVIOR IN LIQUID METAL ENVIRONMENTS

Most LMIE studies focus on tensile testing of embrittlement couples. Fatigue is a more severe test condition, so it may be important to test in fatigue. This is especially important in couples where no embrittlement occurs in tension but may occur in fatigue; since many materials see fatigue loading in actual service conditions; an erroneous conclusion of immunity to embrittlement could be disastrous. For example, smooth specimens of high-purity chromium-molybdenum low-alloy steel (yield stress: ~690 MPa (100 ksi)) are not embrittled by liquid lead, but the same specimens containing a fatigue precrack are severely embrittled by liquid lead. The fatigue life of this steel in liquid lead is reduced to just 25 % of its life in an inert argon environment. Copper-aluminum alloys fatigue tested in mercury exhibit significant endurance limit loss versus those tested in air, with maximum fatigue stress decreasing with increasing grain size [6]. Various nickel alloys, tested in fatigue, all show reduction in fatigue life when tested in mercury compared with results from testing in air. The alloys Nickel 200, Alloy 600, Alloy 800, and Alloy 825 fracture transgranularly when tested in mercury in simple tension, but fractured intergranularly when fatigue tested in mercury, as cracks are able to nucleate at low strain levels due to fatigue loading [12]. Occasionally, fatigue life can actually increase in a liquid metal environment. For example, this phenomenon occurs with steel tested in molten tin at 400 °C. The endurance limit in this case is 90 % higher than in air, due to the formation of the intermetallic compound FeSn_2 during cycling. This compound has a large lattice parameter relative to iron and hence causes high compressive stresses in the surface, resulting in improved life. Reduction in test frequency leads to even larger increases in life, since more FeSn_2 can form in a given time [5].

COMPARISON WITH OTHER FORMS OF EMBRITTLEMENT

Historically, embrittlement phenomena have been divided into four categories: hydrogen embrittlement, stress corrosion cracking, temper embrittlement, and metal induced embrittlement. Many similarities exist between these phenomena, as well as differences. The mechanisms of reduced bond cohesion and reduced bond shear strength are likely at work in HE, SCC, and MIE. HE and LMIE have the same general requirements for occurrence, namely, tensile stress, obstacle to dislocation motion, presence of embrittling species, and low mutual solubility/tendency to form compounds [5]. However, there is generally a greater tendency for plastic deformation ahead of the crack tip with hydrogen, as the small hydrogen atom can readily diffuse into the metal matrix. Liquid metal atoms are too large to diffuse into the crack tip. Consequently, HE fractures tend to be more ductile, with transgranular dimple rupture more common, than LMIE fractures. Crack blunting and even arrest due to plasticity effects is common in hydrogen embrittlement. Nickel alloy Alloy 600 behaves in this fashion. Fatigue life of Alloy 600 actually increases in hydrogen due to hydrogen's promotion of crack tip blunting and work hardening [13]. Alloy 400 is more severely embrittled by mercury than by hydrogen, with crack blunting occurring more readily in hydrogen. Crack initiation is also easier in hydrogen, as the enhanced plasticity of nickel by hydrogen facilitates plastic deformation necessary for crack nucleation [10].

LIQUID METAL INDUCED EMBRITTLEMENT OF NICKEL, NICKEL-BASED ALLOYS, AND AUSTENITIC STAINLESS STEELS

Many similarities exist between nickel and nickel-based alloys and austenitic stainless steels. Both groups are structural alloys with a face-centered cubic crystallographic structure and have similar properties. Both are used when some degree of hostile environment resistance is required. Both are known to be embrittled by liquid mercury [12, 14, 15]. Thus, an overview of embrittlement behavior of nickel and nickel alloys in liquid mercury is appropriate.

LIQUID METAL EMBRITTLEMENT OF NICKEL AND NICKEL-BASED ALLOYS IN SLOW STRAIN RATE TESTING

When Nickel 200, Alloys 400, R405, K500, 600, 625, 718, X750, 800, and 825 were slow strain rate tested in liquid mercury at room temperature, all but the Alloys 800 and 825 were embrittled [14]. All materials were tested in the annealed condition, with grain sizes of 25-50 μm . Surface finishes varied from highly polished to as machined; surface finish did not seem to be a significant variable in the testing. The test specimens themselves were waisted, with a 12.7 mm diameter reducing to 6.35 mm at mid gage length. Gage length was 30 mm. Waisted specimens allow for a stress/strain, and possibly damage, gradient along the gage length as well as a predetermined fracture location without a high initial stress concentration. Strain rate was approximately $1.6 \times 10^{-5} \text{ s}^{-1}$, with some tests performed at additional higher and lower strain rates. As stated above, embrittlement occurred in Nickel 200 and all but the 800 series Alloys; embrittlement did not occur at very high strain rates, where fractures were cup and cone. The degree of embrittlement, as well as the fracture mode, and hence surface appearance, differed from alloy to alloy; strain rate was also a variable in some alloys. When tested in air, all alloys

tested had ductile cup and cone fractures, with microvoid coalescence being the expected fracture mechanism. Strain rate variations in air did not make any significant differences in strength or ductility; FCC metals are typically not strain rate sensitive in air, because the yield strength varies little with temperature or strain rate, and there is no ductile-brittle transition temperature.

Nickel 200 is embrittled by mercury [14]. Reduction in area in mercury is 62 %, versus 84 % in air [16]. An irregular 45 degree slant fracture occurs after the onset of necking. The extent of necking is less than in air; the fracture has multiple origins on the external surface. Many 45 degree markings and cracks are present on the outside of the specimen near the fracture. Fracture is by transgranular shear, with microvoid coalescence taking over in the interior of the specimen. At an order of magnitude slower strain rate, similar fracture topography is evident, again with no intergranular cracking present. Figures 5 and 6 show these various aspects of Nickel 200 fracture [14].

Alloy 400 experiences cup and cone fracture when tested at high strain rates; the reduction in area is similar to that when tested in air. At slower strain rates, fracture is completely intergranular, with a slight (<10 %) reduction in tensile strength [14]. Failure does not occur until well above the yield stress; tensile strength is 530 MPa; yield strength is 250 MPa [16]. Failure is preceded by the development of intergranular cracks at predominately transverse grain boundaries. Figure 7 shows two micrographs of an Alloy 400 fracture [14]. Embrittlement of Alloy 400 by mercury is maximum at approximately room temperature; when tested at a temperature of -30 °C, embrittlement does not occur, presumably due to lack of wetting, and at 80 °C, evidence of lessening embrittlement is present, i.e., a slight recovery in reduction of area, as well as multiple crack origins and less pronounced secondary cracking. This probably is due to the ductility-recovery temperature being approached. RA varies between ~70 % at -30 °C and ~10 % at room temperature. Figure 8 illustrates this trend [7]. Additionally, Alloy 400 shows less embrittlement with increasing amounts of prior cold work, with fractures varying from

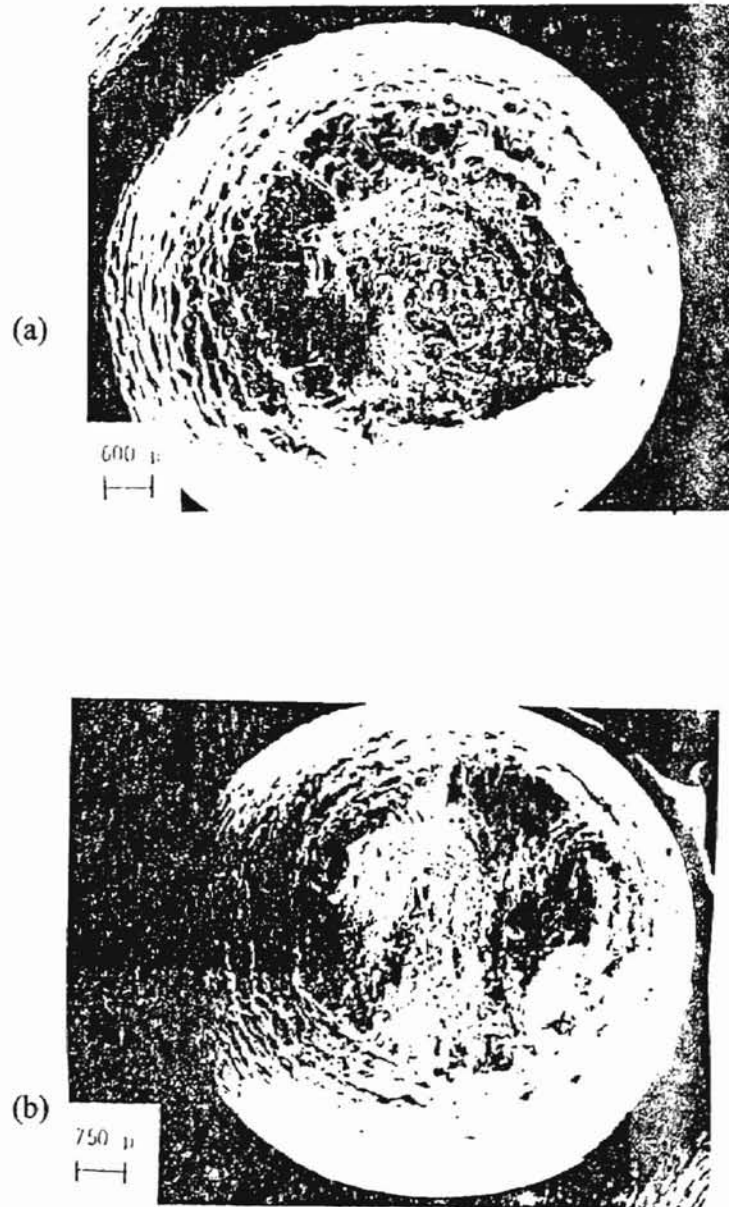


Figure 5. (a) The cup of ductile SSR failure of Nickel 200 in air.
(b) Nickel 200 failure in mercury; slant fracture with several origins, especially at lower edge [14].

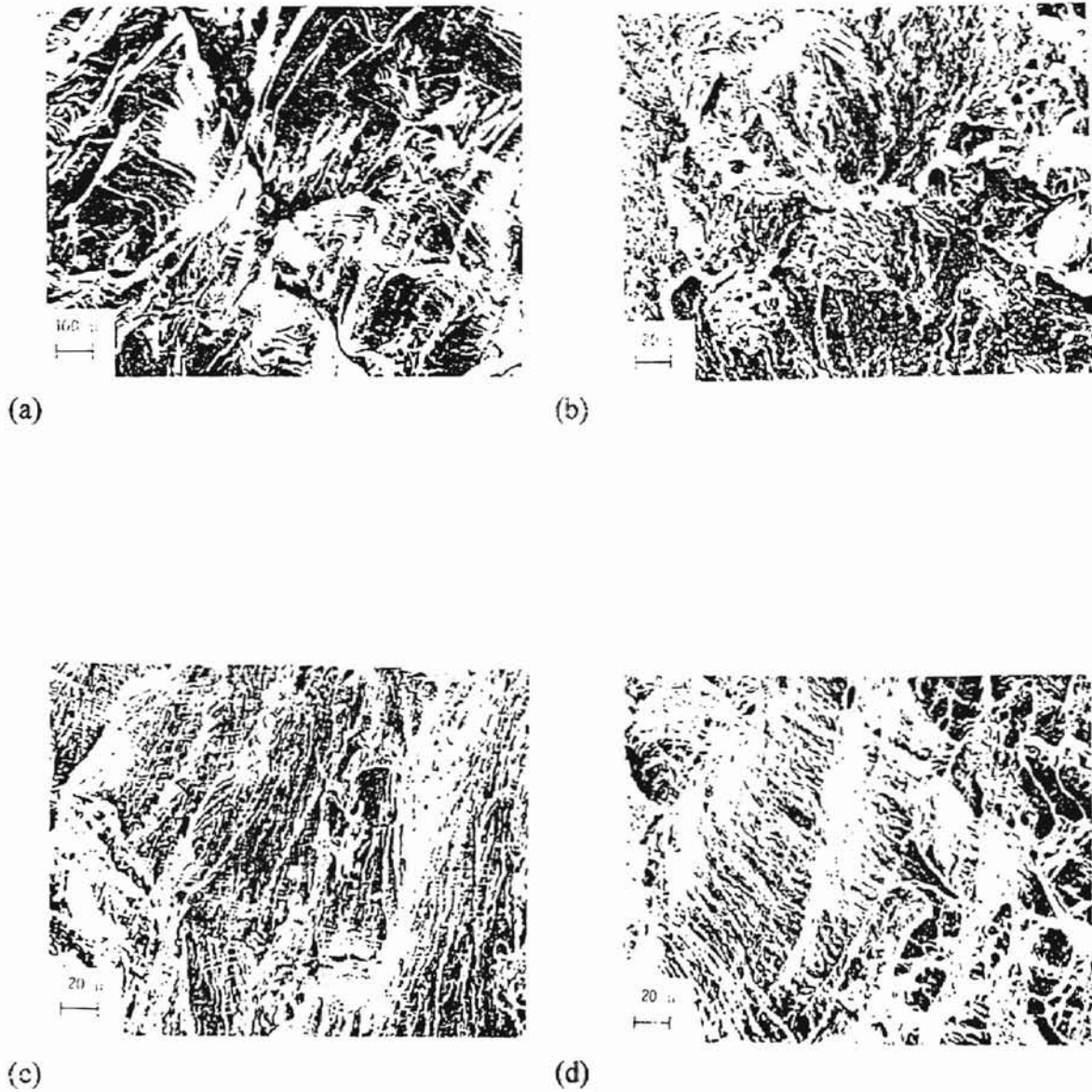


Figure 6. (a) Close-up of necked region of Nickel 200; note intense slip, slant cracking. (b) Origin zone of Nickel 200 fracture; irregular contours, tearing, slip traces evident. (c) Some origin zones on Nickel 200 were more transgranular. Secondary slip traces show clearly. (d) Nickel 200 transition from transgranular to MVC [14].

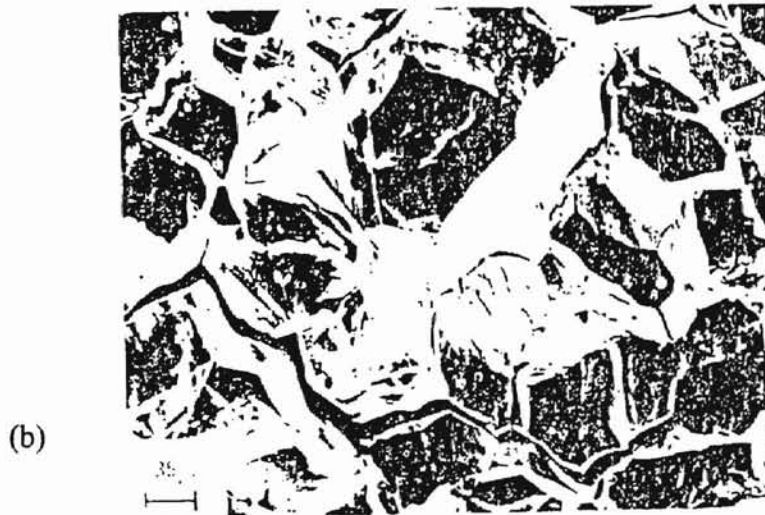
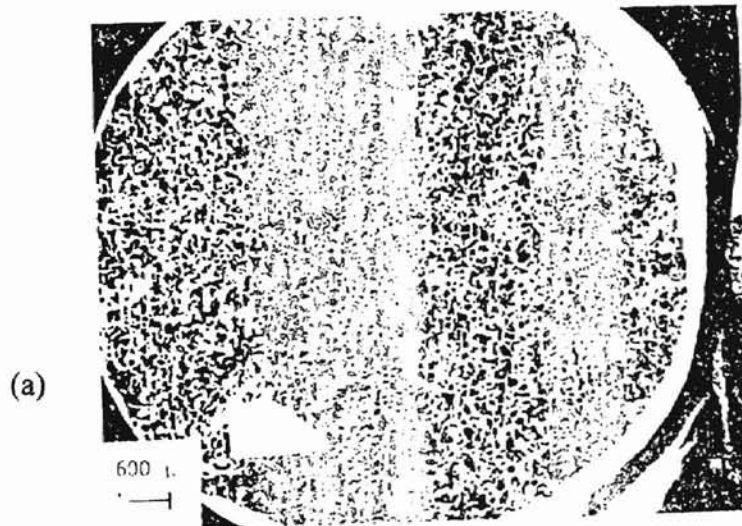


Figure 7. Alloy 400 fractured in mercury. (a) Totally intergranular nature of break.
(b) Close-up of intergranular break, typical throughout cross section [14].

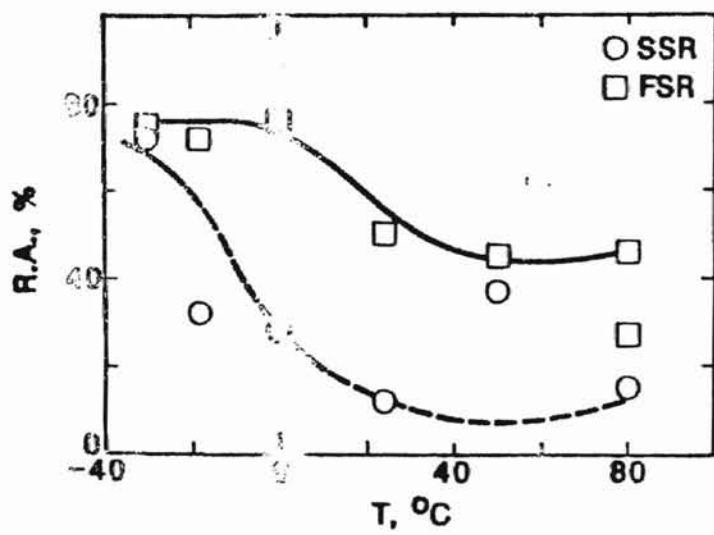


Figure 8. Reduction of area versus temperature, Alloy 400 fractured in mercury [7].

completely intergranular (no prestress, i.e., no prestrain) to predominately transgranular (prestress ~95% of tensile strength). RA correspondingly varies between ~10% and ~30% [9]. In Alloy 400, susceptibility to embrittlement also depends on grain size. The degree of embrittlement rises with increasing grain size, with maximum embrittlement occurring at a grain size of ~250 μm . At this grain size, a reversal of behavior occurs; the degree of embrittlement subsequently drops with further increase in grain size. This is due to the increased ductility of the material facilitated by the larger grain size overriding any embrittlement effects. Strain rate also matters, with higher strain rates producing less embrittlement. At a grain size of 250 μm , embrittlement by mercury does not occur above strain rates of $5 \times 10^{-2} \text{ s}^{-1}$. Increasing strain rate increases the tendency towards transgranular rather than intergranular cracking [10]. Mercury embrittlement of Alloy 400 is also influenced by grain boundary phosphorus concentration. Furnace-cooled specimens, with resulting higher grain boundary concentrations of phosphorus, show twice the per cent elongation as air-cooled samples, 23 % versus 12 % [17].

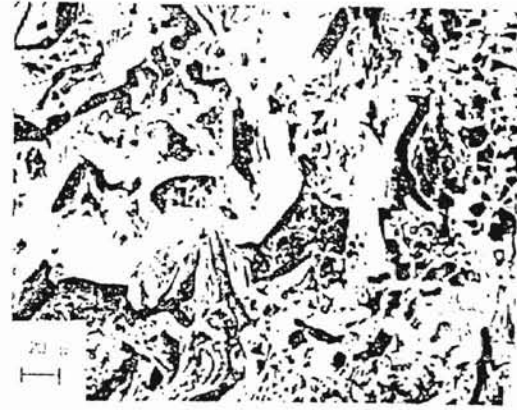
Alloy R405 is the free machining version of Alloy 400. This alloy is less severely embrittled than Alloy 400 in the mercury environment. Fracture is delayed until after necking has begun. The fracture is intergranular, but with tearing, plastic deformation, and signs of dimple rupture towards the center of the specimen. Intergranular side cracks are also evident on this alloy; these cracks are typical of the other Monels and some of the Superalloys. Figure 9 illustrates these fracture characteristics [14].

Alloy K500 is completely embrittled in mercury, with failure occurring before any necking. The fracture surface, like Alloy 400, is completely intergranular, but with some nodular surface irregularities due to second phase particles in the material. Figure 10 shows this fracture surface [14].

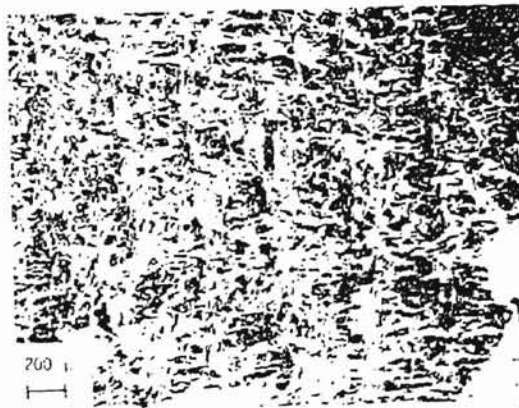
Alloy 600 is embrittled by liquid mercury. No intergranular cracking is present; fracture is almost entirely by microvoid coalescence, with a transgranular region 1 to 6



(a)



(b)



(c)

Figure 9. Alloy R405. (a) Note presence of some necking; no cup and cone, however. (b) In midsection, slip markings, tearing, possible dimple rupture, as opposed to transgranular edge zone. (c) Side view showing extensive surface cracking [14].



Figure 10. Typical fracture surface, Alloy K500. Similar to Alloy 400; note surface irregularities [14].

grains deep around the circumference. Reduction in area at failure is 59 %, versus 63 % in air; so the amount of embrittlement is slight [16]. However, susceptibility to embrittlement is greatly increased when the material is in the sensitized state. Fracture is entirely intergranular in the sensitized state, for cracks can initiate at lower strain levels [18].

Alloy 625 shows no necking in the liquid mercury environment, and fractures in an intergranular manner across the entire cross section. Some grains are seen to have localized nodules and depressions, a la Alloy K500, but the majority of grain surfaces are clean breaks [14].

Alloy 718, which is immune to embrittlement by liquid sodium, is embrittled by liquid mercury. The fracture mode is in between the Nickel 200 and Alloy 400 modes, beginning at the onset of necking, with intergranular flat cracking giving way to MVC and slant fracture towards the center of the specimen. Nodular second phase particles are evident on the grain surfaces in the intergranular origin zone, along with some tearing and slip band traces. At the transition to slant fracture, there is an odd mix of dimpled rupture and intergranular cracking. Figure 11 shows this fracture; note the unusual dimpled/intergranular cracking zone. Alloy X750 behaves similarly to Alloy 625. The intergranular fracture origin zone shows more tearing than typical intergranular fractures; while the entire fracture surface is intergranular, there are more slip lines and tearing across the cross section. Traces of MVC are evident as well. Figure 12 illustrates this behavior [14].

Alloys 800 and 825 are not embrittled in slow strain rate testing in mercury. Cup and cone failures occur after necking. However, numerous 45 degree crack markings on the side of the necked region indicate that these alloys are quite close to the threshold of embrittlement. This lack of embrittlement is shown in Figure 13. An order of magnitude lower strain rate ($\sim 1.6 \times 10^{-6} \text{ s}^{-1}$) does not alter this behavior [14].

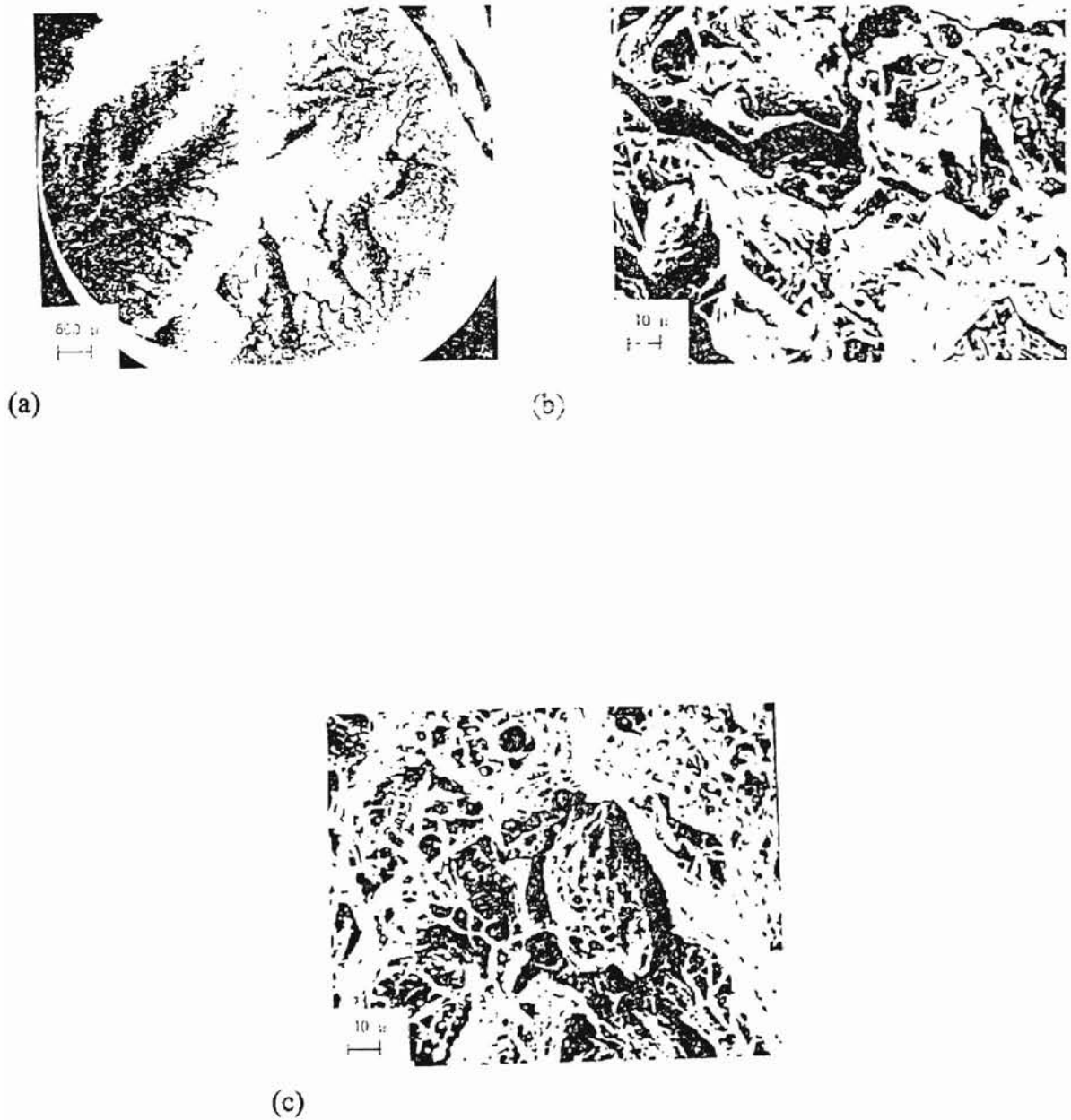


Figure 11. Alloy 718 fracture surface. (a) Mixed mode macroscopic fracture appearance. Mainly flat, with slant zone at top, as viewed. (b) Intergranular origin zone; note second-phase pock-marks. (c) Curious combination of dimple rupture and intergranular separation at transition to slant region [14].

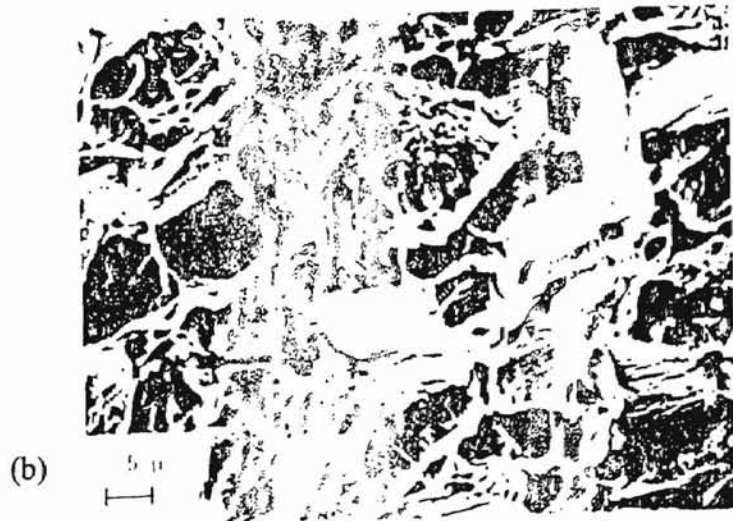
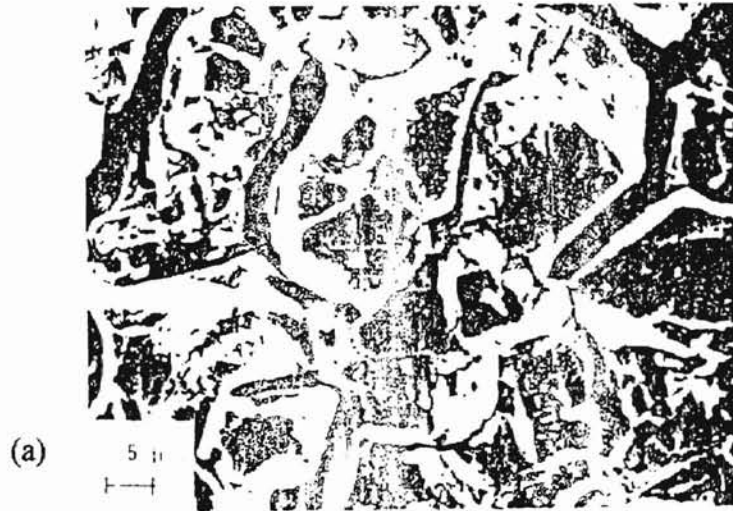


Figure 12. Fracture surface, Alloy X750. (a) Intergranular origin zone with relatively large amount of tearing. (b) Conglomeration of various effects in later stages of fracture

[14].

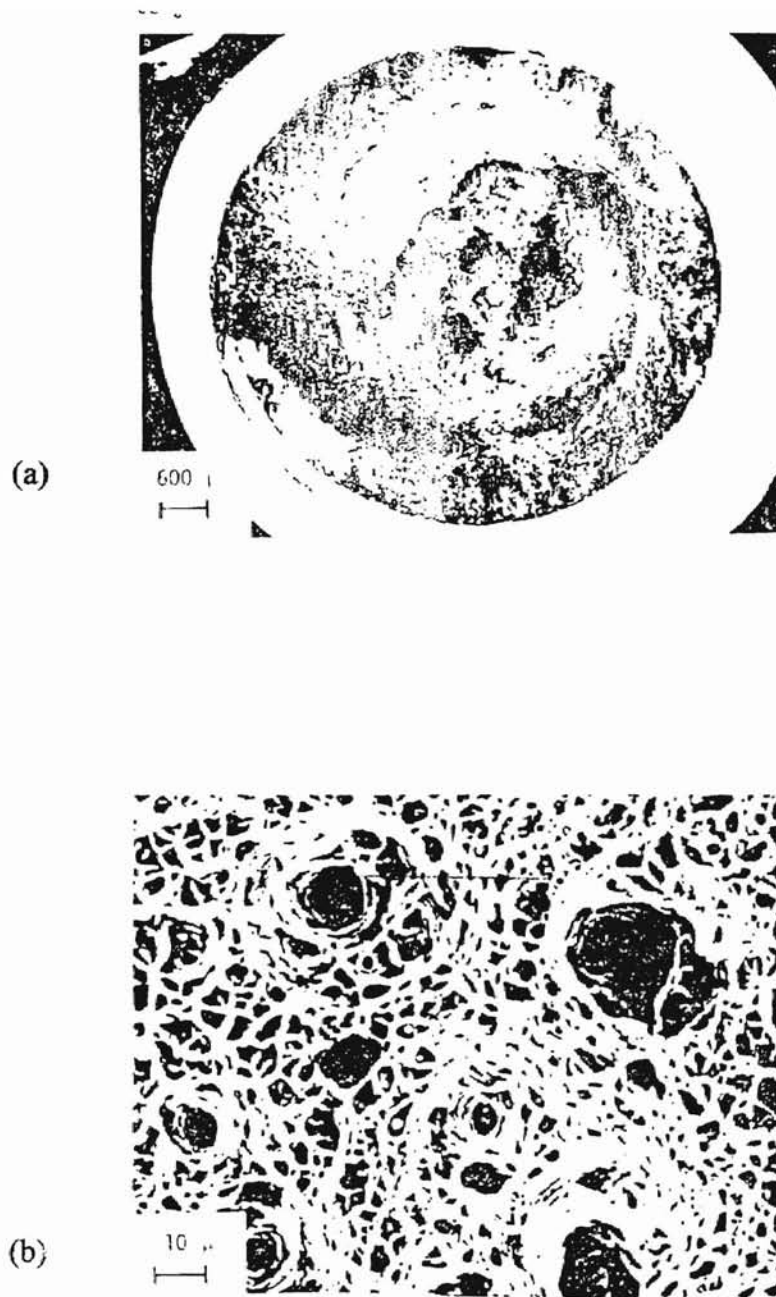


Figure 13. Alloy 800 fracture. (a) Cup and cone fracture. (b) Detail of (a) showing dimpled rupture failure mode. No embrittlement evident; Alloy 825 same [14].

LIQUID METAL EMBRITTLEMENT OF NICKEL AND NICKEL-BASED ALLOYS IN FATIGUE TESTING

When Nickel 200; Monels 400, R405, and K500; Alloys 600, 625, 718, and X750; and Alloys 800 and 825 were fatigue tested in liquid mercury at room temperature, all were embrittled [12]. Specimens were identical to those described in the previous section. In slow strain rate testing, embrittlement was often seemingly limited by high strain levels, sometimes beyond necking, necessary to create a crack. Fatigue testing, however, provides a means by which cracks may initiate well below the tensile strength. For testing, fluctuating tension was used ($R=0$) with a sinusoidal wave form at frequencies of 30-50 Hz. Materials were tested in the annealed and cold worked states at a range of stress levels. The intent was not to develop comparative S-N curves, but to determine the susceptibility to, and mode of, mercury embrittlement [12].

When tested in air, all alloys failed transgranularly; fatigue life was reduced in mercury in all cases. In mercury, major differences in initial intergranular cracking extent and subsequent transgranular cracking existed between the various alloys [12].

Nickel 200 shows a predominately intergranular origin zone with a small minority of grains torn across when tested in the annealed condition in mercury. Next, secondary intergranular cracking occurs, followed by mixed intergranular-transgranular cracking, a brief zone of completely transgranular cracking, and a dimpled rupture final break. Striations do not appear, suggesting a brittle cracking mode. Figure 14 shows fracture surface features of this alloy. Cold-worked Nickel 200 work softens in both air and mercury, when tested at high stress levels, to give cup and cone breaks. For longer-life tests, fracture behavior is similar to that of annealed metal. With the cold worked metal, a greater degree of transgranular tearing in the initial intergranular zone is typical. In air, the fatigue life of annealed Alloy 200 at ~ 0.7 of the tensile strength is ~ 200000 cycles; in

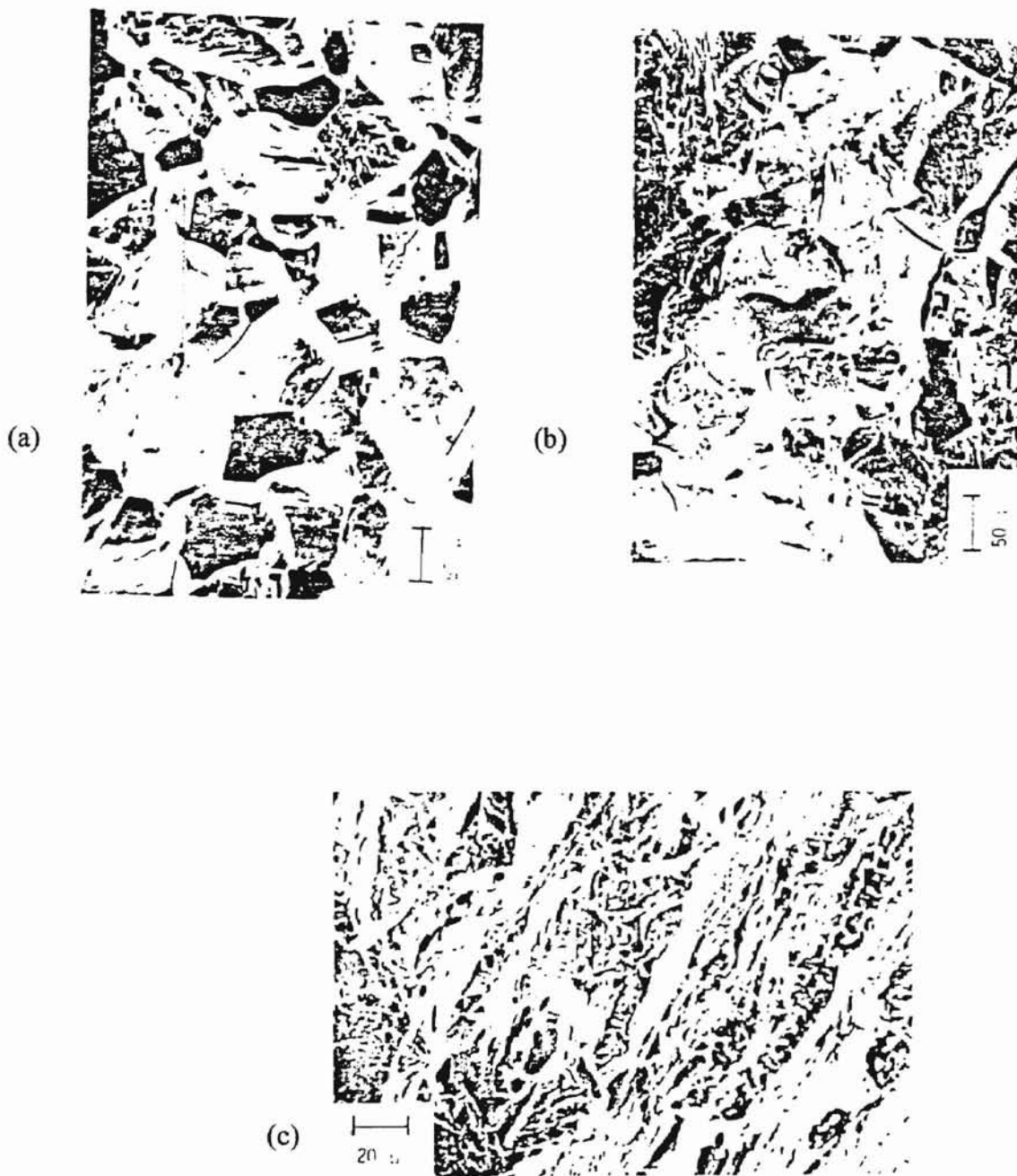


Figure 14. Fracture surface of Nickel 200 fatigued in mercury. (a) Origin zone; note clean grain boundaries, lack of secondary grain boundary cracking, and that some grains are sheared across. (b) Transition region between IG and TG, secondary cracking present. (c) Transition between TG and MVC abrupt overload failure [12].

mercury, the life drops to ~50000 cycles. Similarly, cold-worked Alloy 200 has a fatigue life in air of 265000 cycles; in mercury this figure is reduced to 130000 cycles [12].

Annealed Alloy 400 fails in a completely brittle and intergranular manner. A multitude of surface cracks is typically present; it is as though each grain is separating from its neighbors. Fatigue life at ~0.7 of the tensile strength is ~3500 cycles in mercury; in air, this figure is 300000 cycles. Cold-worked Alloy 400 also shows completely intergranular brittle failure, but with less reduction in fatigue life, 52000 cycles in mercury vs. 200000 cycles in air. Presumably, crack initiation is delayed in this case. At high strain amplitudes, work softening occurs, as in Nickel 200, and cup and cone ductile fracture occurs in both air and mercury. Both high- and low-cycle fractures in mercury show extensive intergranular longitudinal cracking, which does not occur in cold-worked Nickel 200. These cracks can be up to ~ 15 mm long. Figure 15 shows the surface of one such crack. Alloy R405 behaves similarly to Alloy 400, but with a degree of tearing and some traces of shear cracking in later stages of fracture [12].

Alloy K500 is also completely intergranularly embrittled when fatigued in mercury. Side surface cracking and secondary cracking are less than in Alloy 400. Grain boundaries show second phase particles, and no signs of plastic deformation are present. Fatigue life is reduced from ~360000 cycles in air to ~12000 cycles in mercury [12].

Alloy 600 shows a transition from intergranular origin zone to transgranular fracture in the interior of the specimen. Additionally, patches of striations, as well as secondary cracking, are evident. Transgranular tearing of a minority of grains occurs in the origin zone; this feature dominates the later portion of the fracture. Figure 16 shows features of Alloy 600 fracture [12]. Interestingly, intergranular cracking does not occur in slow strain rate testing of Alloy 600 in mercury, unless the material is sensitized [18]. With increasing grain size, the intergranular region is less extensive. Fatigue life decreases from ~110000 in air to ~30000 in mercury at a grain size of 10 μm ; fatigue life decreases



Figure 15. Opened out secondary crack in cold worked Alloy 400; note clean, elongated grains and intergranular cracking in the third orthogonal direction [12].

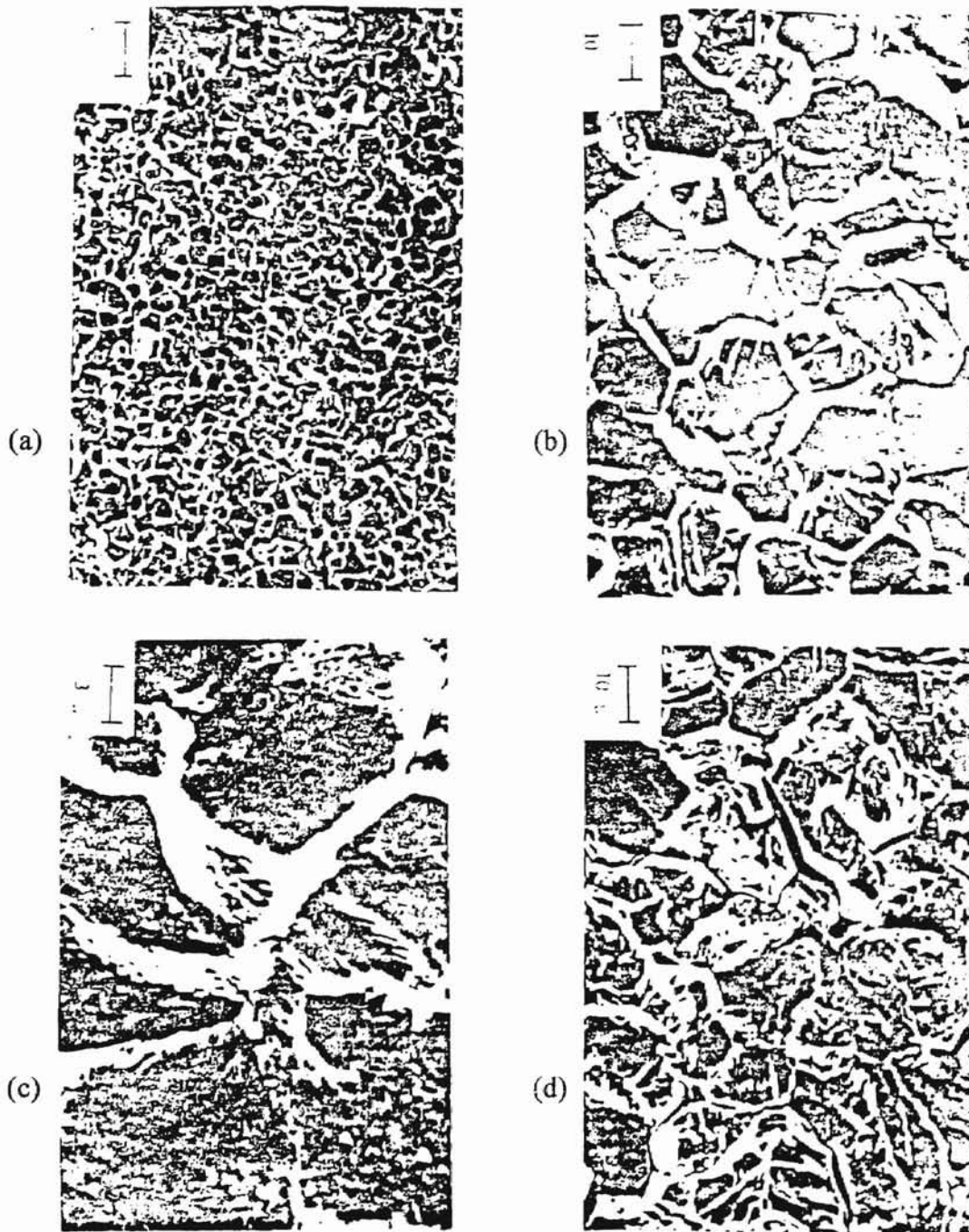


Figure 16. Alloy 600 fracture surface. (a) Predominately intergranular origin zone. (b) Detail of origin zone; note shear failures in minority of grains and occasional secondary cracking. (c) Detail of origin zone; note second phase particles and transgranular fracture of one grain. (d) Later stage of failure; primarily TG, but with some secondary IG cracking [12].

from ~200000 in air to ~55000 in mercury at a grain size of 60 μm . Therefore, while embrittlement may seem to decrease with the reduction of the extent of intergranular cracking at a coarser grain size, the proportional effect on fatigue life is the same [18].

Alloy 625 behaves similarly to Alloy 600 when fatigued in mercury, but with only a trace of intergranular separation at the origin, and the remainder transgranular. Fatigue life is reduced less, from ~400000 in air to ~170000 in mercury.

Alloy 718 shows largely transgranular crack propagation when fatigued in mercury; the fracture texture is flatter and more regular than in air. Occasional intergranular cracking occurs at the origin, with fine striations from the outset. This alloy shows more similarity of fracture appearance in mercury to fracture in air than any other nickel-based alloy. More secondary cracking occurs in mercury, however. Fatigue life is reduced from ~190000 in air to ~75000 in mercury. Figure 17 shows details of Alloy 718 fracture [12].

Alloy X750 shows distinct intergranular cracking in the origin zone, with secondary cracking occurring subsequently. Fatigue life in air is ~60000 cycles; in mercury this figure decreases relatively little, to ~45000 cycles [12].

Alloys 800 and 825 are markedly more affected during fatigue in mercury than are Alloys 600, 625, 718, and X750. While not embrittled by mercury during tensile testing [14], Alloys 800 and 825 are both embrittled in fatigue. Alloy 800 exhibits predominately intergranular failure, with secondary intergranular cracking and transgranular shear occurring in late stages of failure. Alloy 825 also fails intergranularly, but with more transgranular cracking and possible striations occurring. Alloy 800's fatigue life decreases from ~290000 cycles in air to ~20000 cycles in mercury; Alloy 825 shows a decrease from ~170000 cycles in air to ~30000 cycles in mercury. Figure 18 shows example fracture surfaces of these alloys [12].

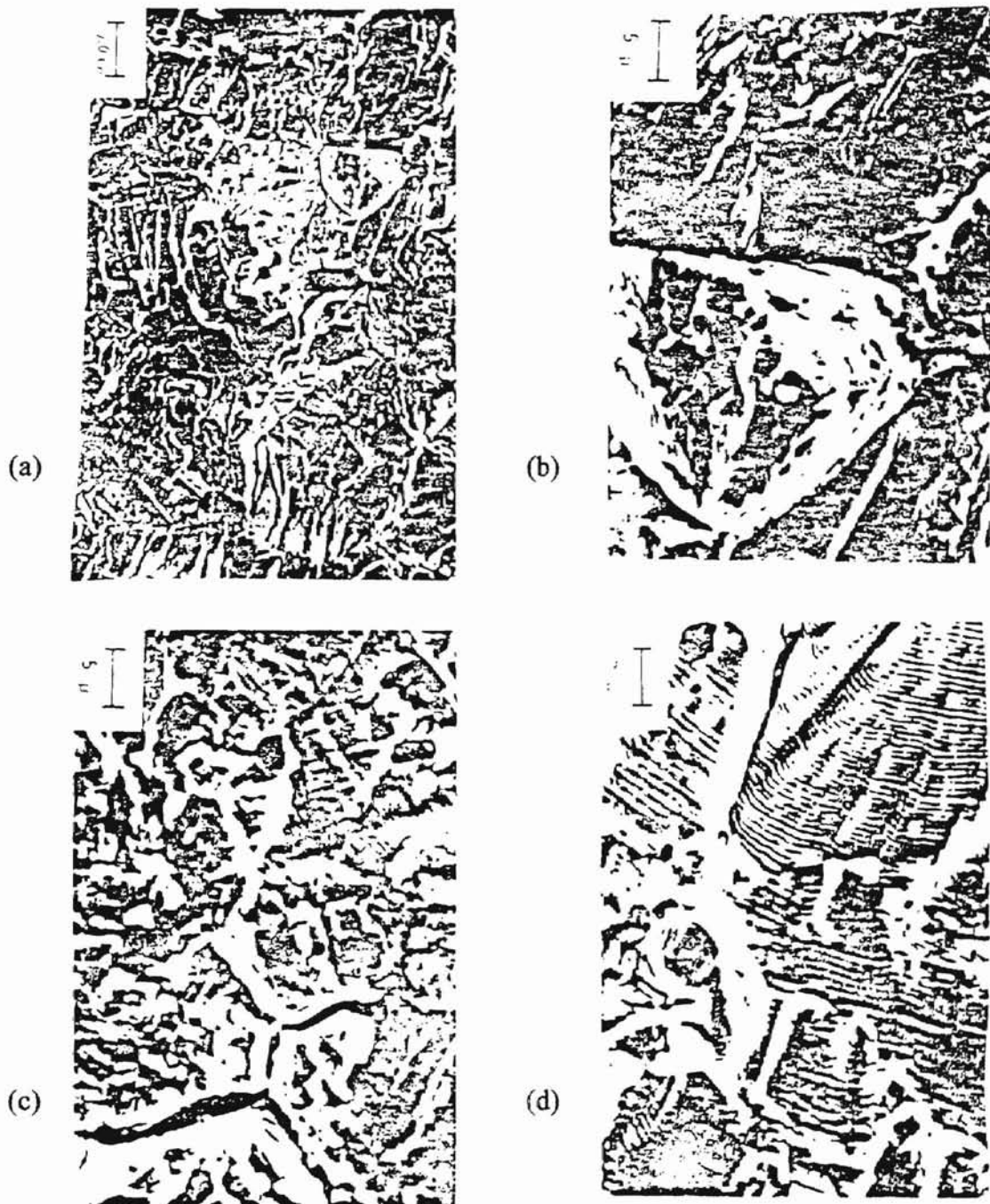


Figure 17. Alloy 718 fatigue fracture in mercury. (a) Transgranular cracking with traces of intergranular cracking. (b) Detail of (a) showing individual grain; note slip, or possible striation, markings on surrounding grains. (c) Intermediate stage of failure; note extensive secondary cracking of IG and TG nature. (d) Late stage of failure; note well defined striations and minimal secondary cracking [12].

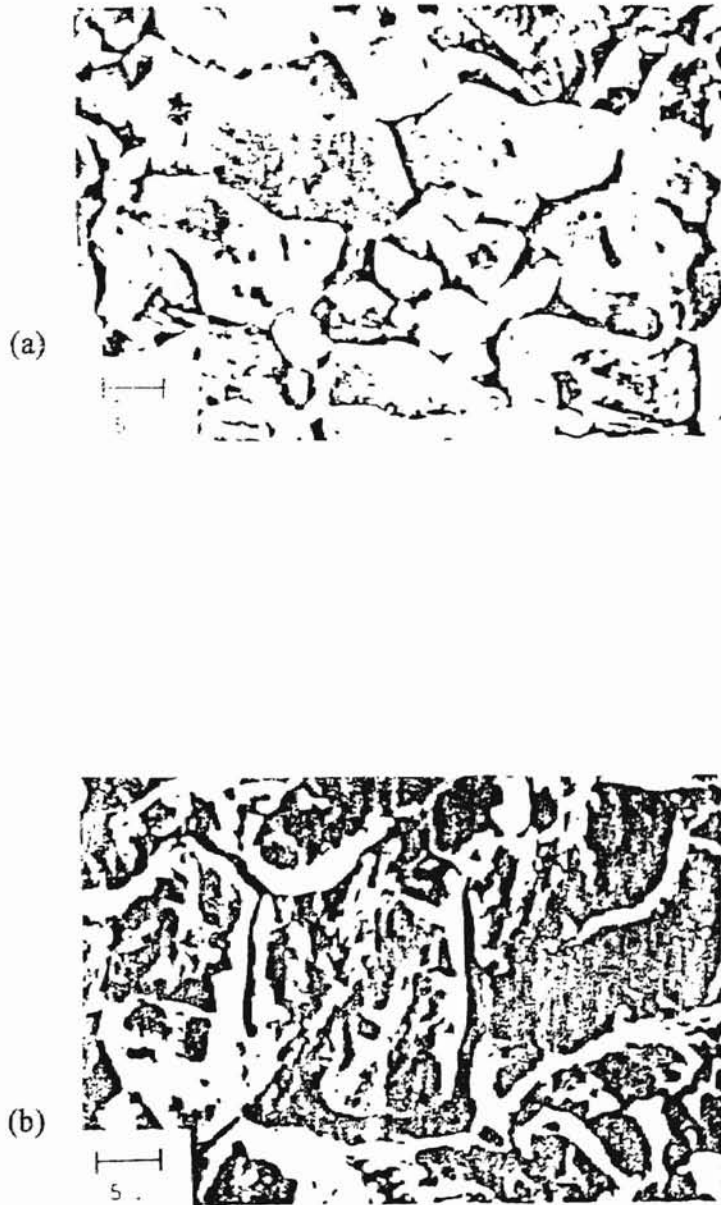


Figure 18. Fracture surfaces of (a) Alloy 800 and (b) Alloy 825. (a) Fatigue origin zone, primarily IG. (b) Fatigue origin zone, mixed mode cracking and slip, or possibly striations

[12].

LIQUID METAL EMBRITTLEMENT OF TYPE 304 STAINLESS STEEL

There seems to have been one previous study of LMIE of AISI Type 304 by liquid mercury. Type 304 stainless steel is embrittled in liquid mercury during slow strain rate testing [15]. When tested at room temperature in air, reduction in area is ~80 %. When tested in room-temperature mercury, reduction in area is ~40 % at strain rates lower than $1 \times 10^{-4} \text{ s}^{-1}$. Figure 19 shows a typical specimen. At a strain rate of $3.3 \times 10^{-3} \text{ s}^{-1}$, reduction in area climbs to ~44 %; at 8.3×10^{-3} , this figure is ~63 %. Heat-to-heat material variations, as well as specimen diameter, have negligible effect on embrittlement. Embrittled specimens show secondary cracking along their entire gage lengths (cylindrical specimens). These secondary cracks are perpendicular to the specimen axis. They are transgranular, shallow, and blunted from localized plastic strain preceding crack arrest. Fractures are composed of faceted, extensively branched brittle outer regions surrounding flat regions of ductile fibrous rupture. Brittle fracture occurs over 50 % the cross-sectional area of specimens tested at strain rates of $1 \times 10^{-4} \text{ s}^{-1}$, at higher strain rates, less brittle cracking occurs. At $8.3 \times 10^{-3} \text{ s}^{-1}$, fracture occurs primarily by ductile rupture, with necking likewise occurring, and only small regions near the surface exhibiting brittle LMIE fracture characteristics. Figure 20 shows fracture surfaces of Type 304 tested at various strain rates. The embrittled outer regions consist of transgranular and intergranular cracking, while the inner regions fracture by microvoid coalescence, and hence have a dimpled fracture appearance. Figure 21 shows these two regions.

DISCUSSION

The nickel alloys rank in susceptibility to embrittlement, most to least, as follows: 400, K500, 625, R405, X750, 718, 600, 200, 825, 800 [14]. This order does not take into

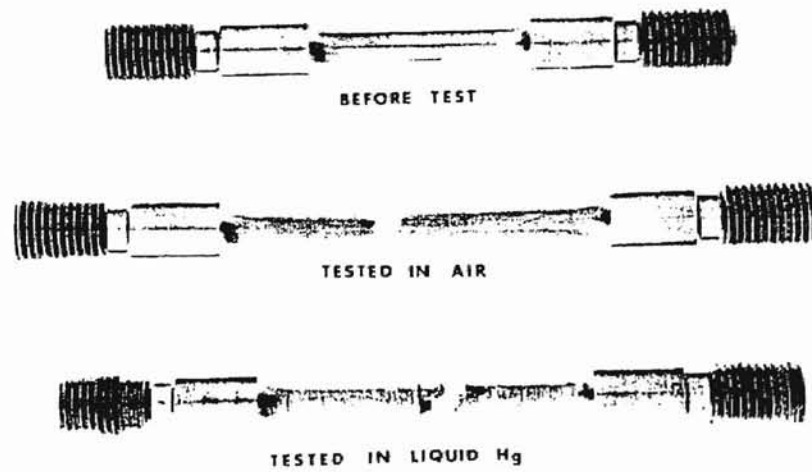


Figure 19. Typical Type 304 test specimen [15].

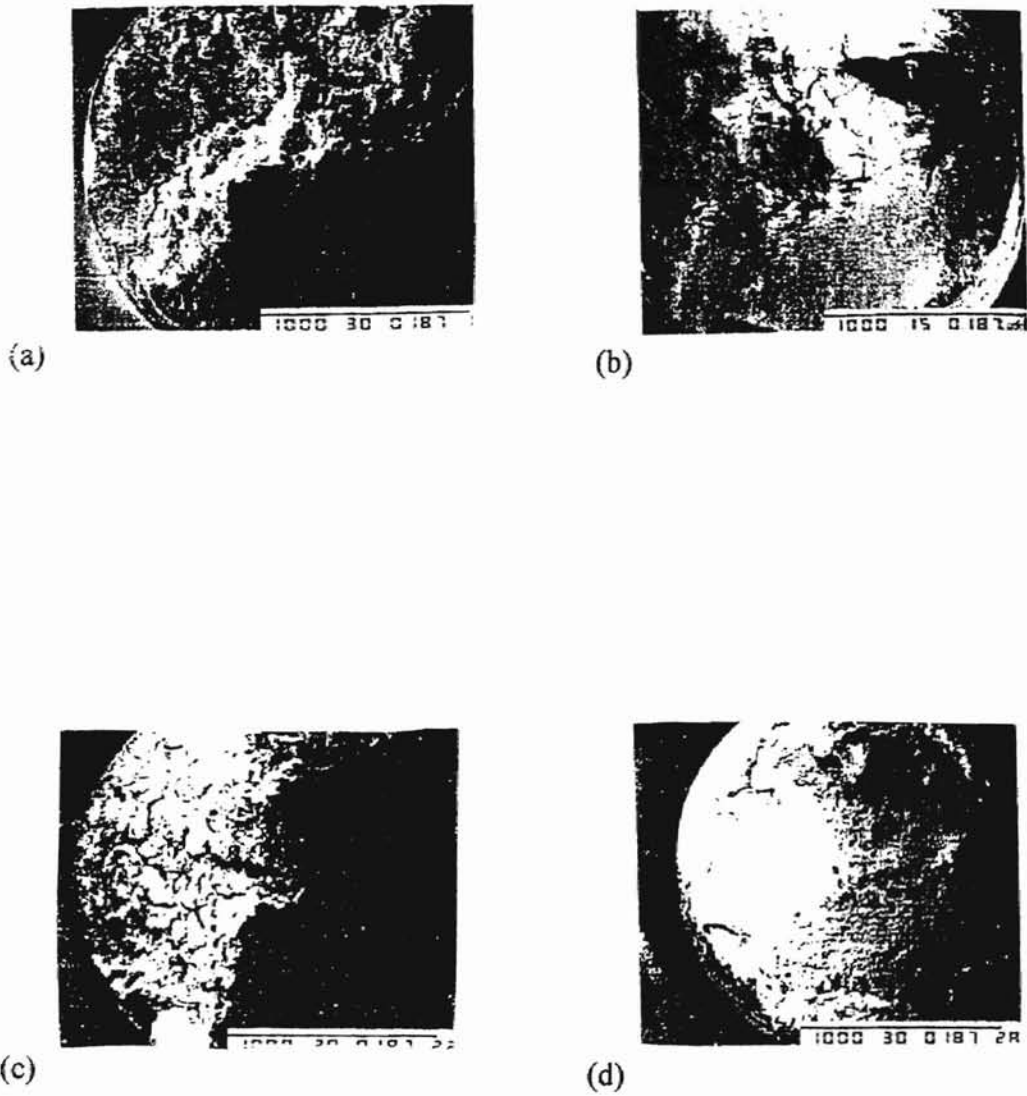


Figure 20. Fracture surface of Type 304 at varying strain rates. (a) $5 \times 10^{-7} \text{ s}^{-1}$, (b) $1 \times 10^{-4} \text{ s}^{-1}$, (c) $3.3 \times 10^{-3} \text{ s}^{-1}$, (d) $8.3 \times 10^{-3} \text{ s}^{-1}$ [15].

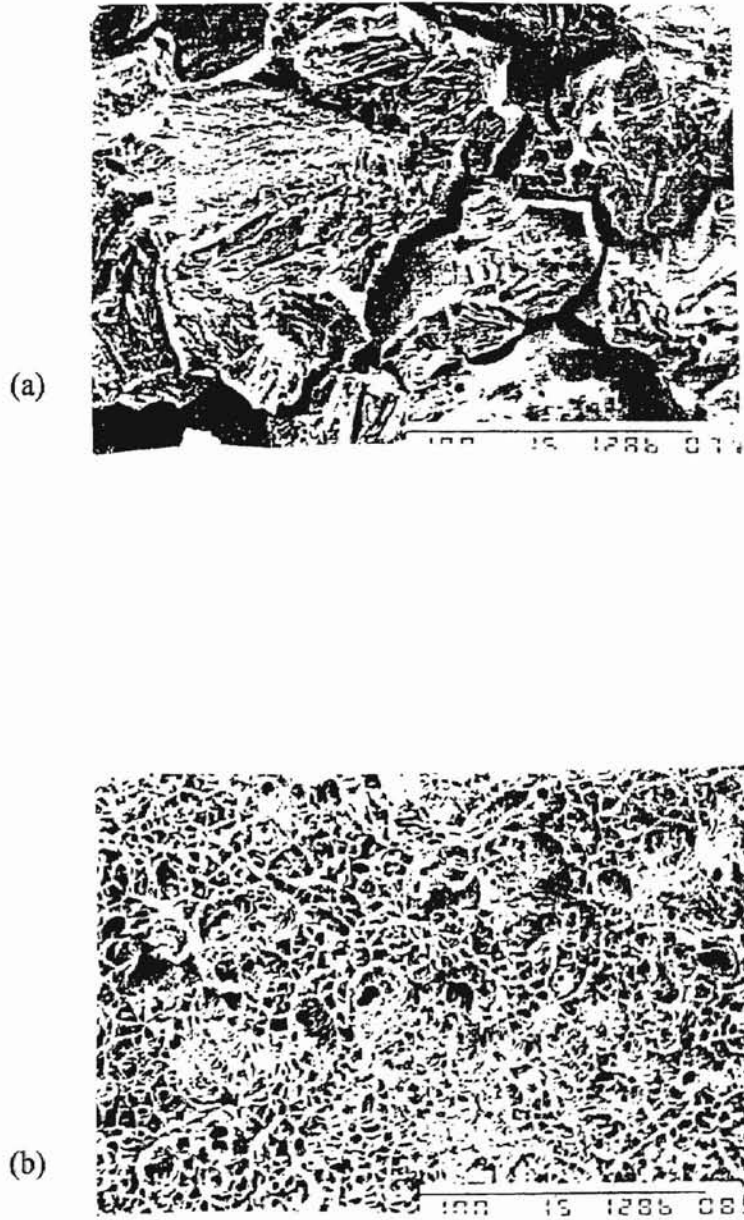


Figure 21. Fracture surface of Type 304 tested in mercury at $5 \times 10^{-6} \text{ s}^{-1}$. (a) Embrittled outer region. (b) Ductile central region [15].

account sensitization effects with Alloy 600. There is no correlation of this order with stacking fault energy, tensile strength, presence or absence of second phase particles, or ductility. Embrittlement of these alloys is influenced by grain size; for example, Alloy 400 is more embrittled at fine grain sizes due to embrittlement being nucleation limited. At coarser grain sizes, embrittlement becomes propagation limited, due to ready plastic deformation of surface grains and hence ready crack blunting. At still coarser grain sizes, plastic deformation is too great to allow cracks to even initiate [10]. Embrittlement of these alloys is also influenced by temperature; Alloy 400 shows a typical maximum of embrittlement near room temperature [7]. Strain rate also matters, with susceptibility increased at slower strain rates [10]. Strain rate also affects Type 304, with less embrittlement occurring at higher strain rates [15]. Additionally, prior cold work affects degree of embrittlement; Alloy 400 is less embrittled with increasing prestrain [9]. Interestingly, those alloys high in iron seem to be less embrittled by liquid mercury [14]. Perhaps relevant to the present study, Alloys 800 and 825, nickel-iron-chrome alloys, are embrittled relatively little in slow strain rate testing; this trend may explain the relatively minor embrittlement of Type 304 in slow strain rate testing [15]. The question of whether embrittlement of Type 304 is increased in fatigue testing, as occurs with the 800 series nickel alloys, remains unanswered. An additional relevant issue is the question of Type 304's embrittlement behavior when sensitized. Like Alloy 600, Type 304 can be sensitized by heating in a certain temperature range, inducing the nucleation and growth of chromium carbides along grain boundaries, which causes grain boundary chromium depletion [18, 19]. Presumably, Type 304 will exhibit an increase in embrittlement akin to that of Alloy 600 when sensitized.

CHAPTER 3

PROPOSED STUDY

This study further investigates the liquid metal embrittlement phenomena of Type 304 stainless steel by liquid mercury. Both slow strain rate and fatigue testing are utilized. Insofar as results of embrittlement studies of nickel-base alloys in liquid mercury can be generalized to the mercury embrittlement of Type 304, and taking into consideration the previous work on Type 304, the following results may be anticipated:

- 1) Strain rate will likely not have a great effect on embrittlement, except at high strain rates
- 2) Embrittlement can be expected to be more severe in sensitized samples
- 3) Embrittlement will likely increase with increasing grain size
- 4) Embrittlement will likely decrease with prior cold work
- 5) A higher degree of embrittlement may occur in fatigue, versus slow strain rate, testing
- 6) Wetting is likely induced by strain at high energy sites

The purpose of this study is to use Type 304 stainless steel, the most widely used commercial austenitic stainless, to examine the effect of the above variables on LMIE. It is anticipated that of the nickel base alloys, the closest affinity will be to Alloy 800, due to the similarity of composition of these two alloys:

Table I. Nominal Chemical Composition of N80000 and S30400

Alloy	composition, w/o									
	Fe	Ni	Cr	C	S	Si	Cu	Al	Ti	P
800	43.85	32.28	21.23	0.07	0.001	0.35	0.34	0.46	0.38	--
304	71.12	8.30	18.58	0.06	0.024	0.50	--	--	--	0.030

The study will begin with the initial characterization of the material. The as-received condition will be ascertained, as well as grain sizes resulting from heat treatment. Sensitization of the material will be induced, and subsequently verified. Hardness of the material in these various conditions will be recorded. Slow strain rate testing will be conducted to test embrittlement versus strain rate, sensitization, grain size, and prior cold work. Fatigue testing will be conducted to determine the effect of fatigue loading on LMIE of Type 304. Specimens tested in mercury will be cleaned, and the results of testing will be analyzed with stereoscopic zoom microscope (SZM) as well as scanning electron microscope (SEM) techniques.

CHAPTER 4

EXPERIMENTAL PROCEDURE

MATERIAL

Specimens were machined from two 12-ft. rods of 0.5-in diameter bar stock; these had differing as-received conditions. The first batch had a hardness of ~98 HRB, with a grain size of 100-150 μm ; the second had a hardness of ~27 HRC and a GS of 25-35 μm . Additionally, some degree of sensitization was evident in the second batch, as-received.

HEAT TREATMENT

For testing of annealed material, the first batch was annealed for 1 hour at 1000 °C; grain size was unchanged, and hardness dropped to ~82 HRB. The same treatment of second-batch specimens also yielded no grain growth, with a drop in hardness to ~82 HRB. This drop in hardness with constant grain size after annealing suggests the high initial hardness was due to the as-received bar being rather heavily cold-worked. As initial testing was performed with the first batch, heat treatment was necessary to get the second batch's grain size within the range of the first batch's. Annealing at 1150 °C for 10 minutes, followed by water quenching to prevent sensitization upon cooling, accomplished this objective. Additional specimens were annealed for 20, 30, and 60 minutes at this temperature to produce grain sizes of 200-350, 250-400, and 300-500 μm , respectively. Annealing a second-batch specimen for 1 hour at 1230 °C also produced a grain size of 300-500 μm , suggesting that perhaps a grain-growth limit has been reached. Heat treatment to induce grain growth was initially based on a chart from the US Air Force Structural Alloys Handbook [20]. Actual grain growth experienced in this research was

much greater than that predicted by this graph. Figure 22 shows the reference chart as well as a graph of grain-growth results in this research. Sensitization was induced by treating specimens at 700 °C for 3-4 hours, followed by air cooling, although it was subsequently found that sensitization could be induced at this temperature in much shorter times, 1 hour being quite adequate for full sensitization [19].

POLISHING AND ETCHING

For both grain size and sensitization analyses, metallographic examination of the material was required. Polishing was performed by mechanical means, with successive sandpaper grinding at 240, 320, 400, and 600 grits, followed by polishing on cloth wheels impregnated with alumina of successive 1000 grit, 5, 3, 1, and sometimes .3 and .05 μm sizes. Satisfactory results were generally realized with a final polish at the 1 μm level. Unsatisfactory results occur when a polishing step is skipped; the addition of the 1000 grit polishing step greatly improved results. For grain size determination, except in the case of sensitized specimens, specimens were etched with a mixture of 10 mL nitric acid, 10 mL acetic acid, 15 mL hydrochloric acid, and 2-5 drops of glycerin [21]. The ASM recommends that this etchant may be used either by immersing the specimen or by swabbing; it was found that immersion produced unacceptable and unreadable results in this case; satisfactory results were produced by swabbing. As Type 304 deforms quite readily due to its low stacking fault energy, the material would appear to be easy to polish. However, it is actually quite difficult to produce satisfactory results, as layers of mechanical deformation resulting from polishing can obscure the true microstructure. Consequently, the polishing process must be carefully performed; skipping steps (such as the inadvertently skipped 1000 grit step in this case) will likely produce unacceptable results. Similarly, the choice of etchant/technique is quite sensitive; the nitric/acetic/hydrochloric/glycerin etchant was first rejected due to unacceptable results

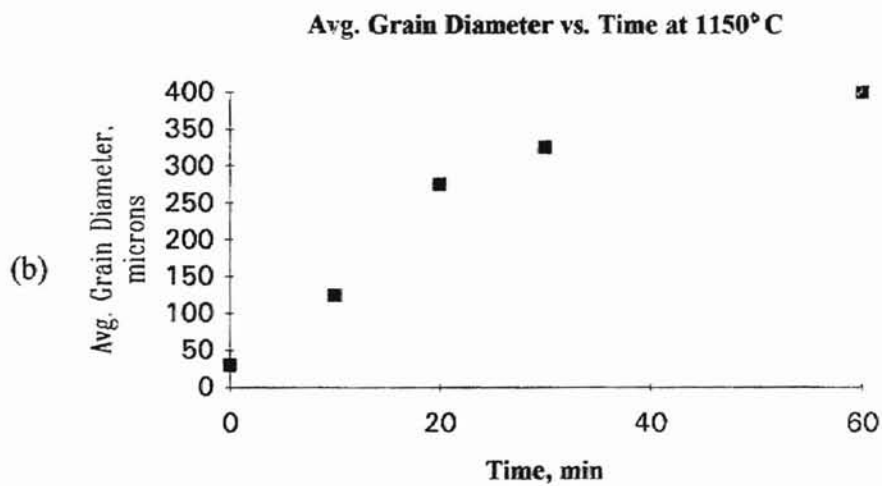
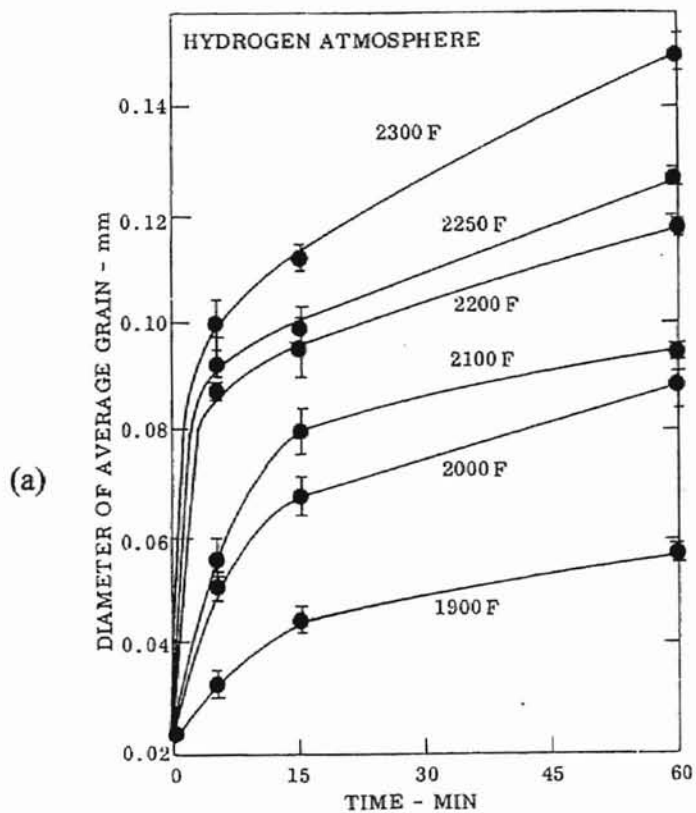


Figure 22. Grain growth vs. time. (a) Reference chart [20]. (b) Experimental results.

when specimens were immersed. Only later experimentation with swabbing and this etchant produced acceptable results. The testing for sensitization (and for grain sizes in sensitized specimens) was performed with electrolytic etching in oxalic acid solution, as per ASTM specifications [22]. Specimens were etched at 1 A/cm^2 for 1.5 min in 10% oxalic acid solution. Sensitized specimens take on a distinctive ditch appearance at the grain boundaries; unsensitized specimens have a characteristic step appearance at the grain boundaries. Figure 23 shows these typical appearances.

GRAIN SIZE DETERMINATION

Grain sizes were determined by photographing the microstructures with a Polaroid microscope-mounted camera and measuring representative grains directly. Photographs were taken of a 1-mm scale for reference. Photographs had a final magnification of $100\times$ and $400\times$.

SPECIMEN PREPARATION

Waisted specimens were used for this series of experiments. These were machined from the bar stock, reducing gradually to 0.25 inch at mid-gage length. Gage length was nominally 1.2 inches. Specimens were 6 inches in total length. Waisted specimens allow for a stress/strain, and possibly, damage, gradient along the gage length. They also facilitate a predetermined location of fracture without a high initial stress concentration. Figure 24 shows the specimen dimensions in detail. Samples were prepared for testing by subsequent polishing with 240, 320, 400, and 600 grit sandpapers. The last polishing step was performed longitudinally to insure that no lateral defects existed to aid in cracking of the material when tested. Specimen gage lengths were cleaned with hydrochloric acid to remove tarnish, facilitating wetting by the liquid mercury.

(a)



(b)



Figure 23. Typical microstructural appearance of (a) unsensitized (Step Structure) and (b) sensitized (Ditch Structure) stainless steel [22].

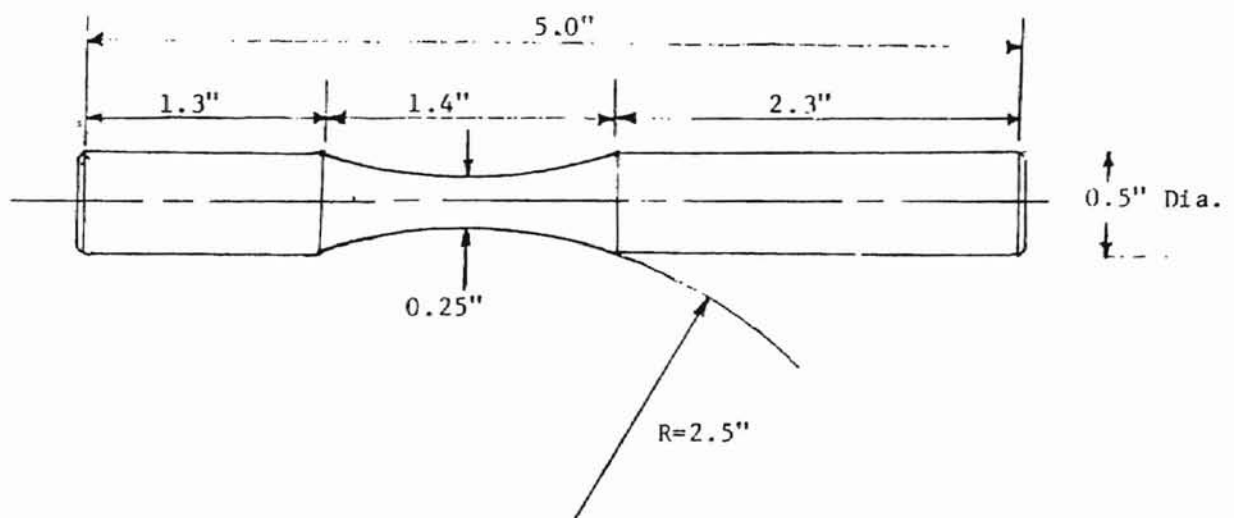


Figure 24. Specimen dimensions (actual total length 6 in.).

TESTING

All testing was performed on an MTS machine. For slow strain rate testing, displacement control was utilized to test specimens at ram displacement rate of 6×10^{-6} in·s⁻¹, yielding a strain rate of $\sim 3 \times 10^{-5}$ s⁻¹, except where strain rate was the variable. Strain rate was computed by assuming a 0.2 in effective gage length due to the waisted specimen geometry, and by assuming a constant strain rate with constant ram motion. These assumptions allowed the use of the definition of engineering strain to compute the amount of strain for a given time period, and hence the strain rate. Strain rates of $\sim 3 \times 10^{-4}$ and $\sim 3 \times 10^{-3}$ s⁻¹ were also tested. Specimens were loaded at a higher ram displacement rate ($\sim 1 \times 10^{-3}$ in·s⁻¹) to just under the yield strength; the test was then allowed to proceed at the slow strain rate. This procedure was followed to prevent an unnecessarily long amount of time being spent on each test; as no embrittlement occurs before yielding, there was no point in reaching the yield stress at the slow strain rate. Several previous workers have shown that hold periods under load produce no crack initiation or increase in embrittlement.

Fatigue testing was performed under load control. Alternating tension with a sinusoidal wave input was used; R=0.1 was used to prevent compression in the specimen.

For tests in mercury, a plastic cup surrounding the specimen was filled with triple-distilled mercury; a lid was then placed over this cup. The entire assembly was contained within a plastic bag to contain any unlikely spillage. Figure 25 shows the apparatus used for testing in mercury.

After testing in mercury, the mercury was removed from the fracture surfaces by ultrasonically cleaning in a mixture of 4 parts Micro (a commercial cleaning solution) and 1 part concentrated nitric acid. Mercury removal was much more easily performed if the mercury was removed immediately following testing; the nitric acid could in fact be left out of the cleaning solution for cleaning freshly broken fracture surfaces. Additionally,

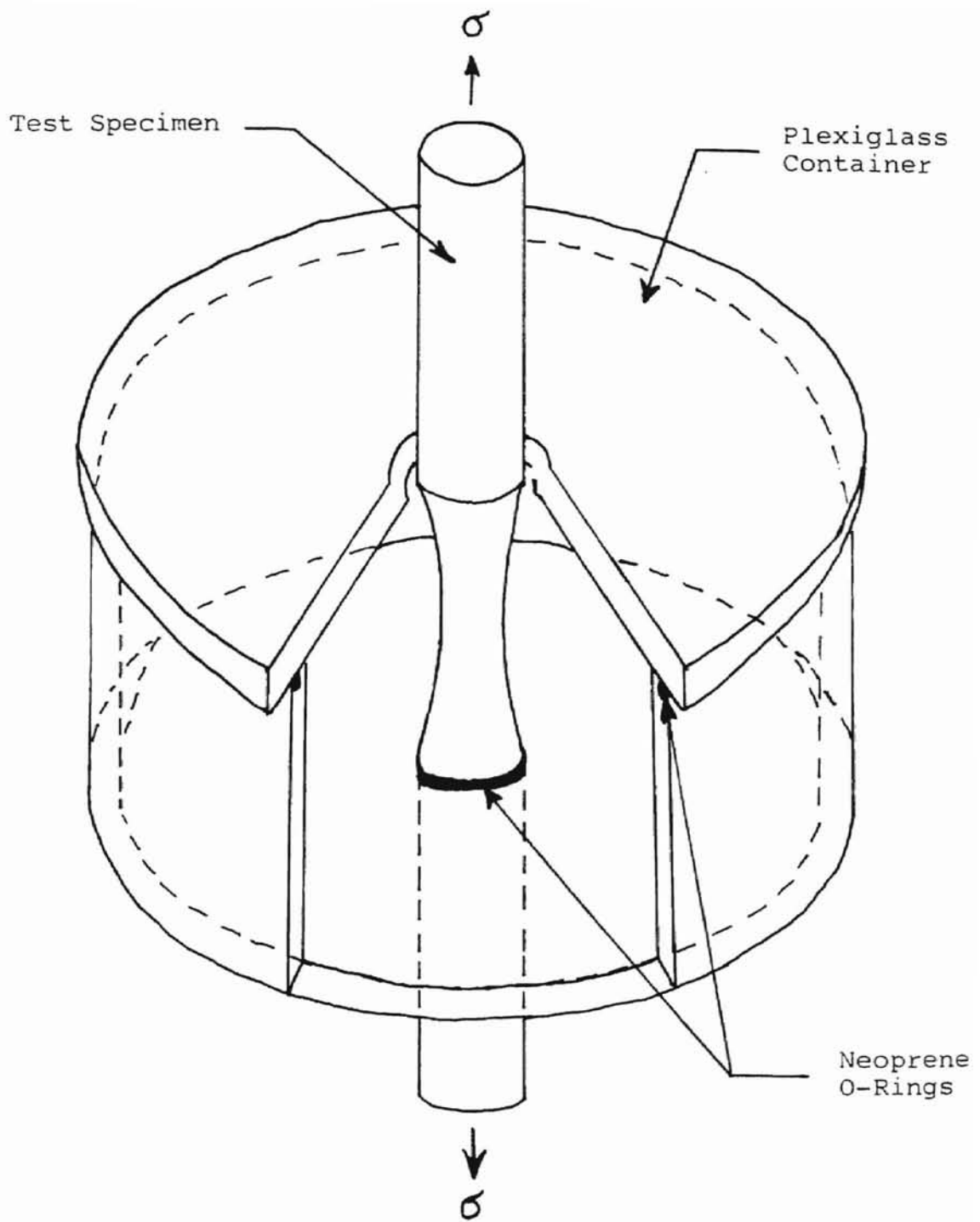


Figure 25. Apparatus for testing in mercury.

brushing the specimen with a nylon brush during ultrasonic cleaning seemed to assist mercury removal.

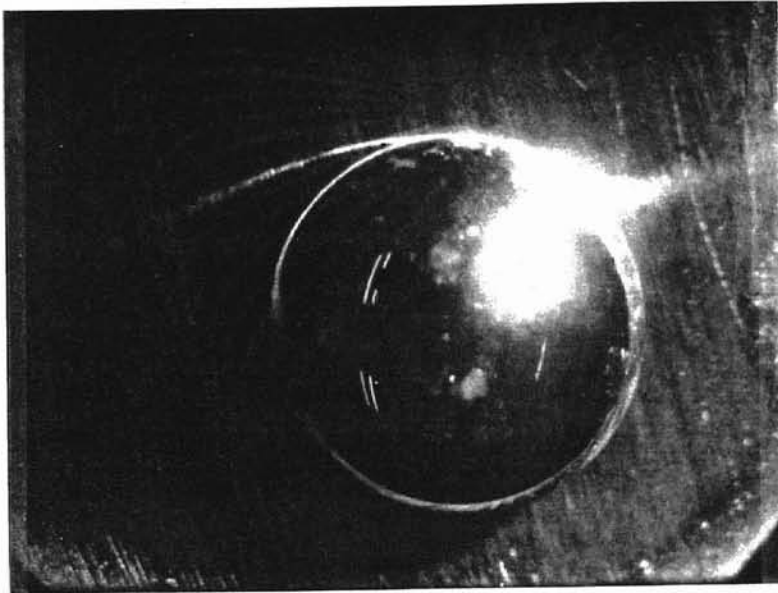
MICROSCOPY

Fracture surfaces were then analyzed using SZM and SEM microscopy. The SZM was used simply to identify potentially interesting specimens for SEM analysis, as well as to inspect mercury cleaning results on the fracture surfaces. SEM analysis was performed to determine the mode of cracking in the various fractures, as well as to examine the extent of secondary and side cracking, where applicable.

WETTING

Wetting behavior does not occur in unstressed specimens. Photographs were taken in the SZM to verify this nonoccurrence of wetting. The surface used for this test was polished to a 600 grit finish; while cleaning of the surface with hydrochloric acid was omitted for this photo, subsequent examination of a surface so cleaned showed identical non-wetting characteristics. Additionally, a few spherical drops of mercury were noted adhering to the fracture surface of one of the specimens when viewed in the SEM. Generally, such drops were found adhering to the surface in crevices and similar hard-to-reach locations when the specimens were analyzed under the SZM during cleaning. Figure 26 shows these unwetting drops. When the SZM photo was taken, tilting the specimen to attempt to better expose the spherical nature of the drop's interface with the surface simply resulted in the drop rolling off of said surface. This occurrence underscores the nonwetting nature of the mercury/steel interface.

(a)



XX sessile drop on 600 grit surface

(b)



Figure 26. Unwetting drops of mercury on (a) 600-grit polished surface (SZM) and (b) fracture surface (SEM, 100 \times).

CHAPTER 5

RESULTS

INITIAL RESULTS

The material was tested in the as-received condition in air to establish baseline data. This test was performed at a high strain rate, as FCC materials are not strain-rate sensitive outside of an embrittling environment. Additionally, an as-received specimen was tested at a slow strain rate in mercury, as was an annealed specimen. The pertinent data from these tests are given in Table II.

Table II. Baseline Data

condition	strain rate (s ⁻¹)	grain size (μm)	hardness (HRB)	σ_{Fmax} (ksi)	red. of area (%)
as rec., air	6.0×10^{-3}	100-150	98	132	78
as rec., Hg	3.0×10^{-5}	100-150	98	132	40
annealed, Hg	3.0×10^{-5}	100-150	82	114	43

As can be seen from the table, the air-broken specimen had a typical (~80 %) high reduction of area figure for Type 304 [20]. This specimen was necked, with a classical cup/cone fracture. In mercury, the reduction of area was markedly lower for both as-received and annealed specimens. Both specimens were not necked, with jagged irregular fractures. SEM examination revealed that the air-broken specimen fractured, as expected, solely by microvoid coalescence. Figure 27 shows this fracture surface. The microvoid sizes, and irregularity thereof, as well as the secondary cracking, are akin to similar photographs in reference books [23]. In mercury, the as-received material fractured generally transgranularly, with a small bit of MVC at the fracture terminus. Many slip

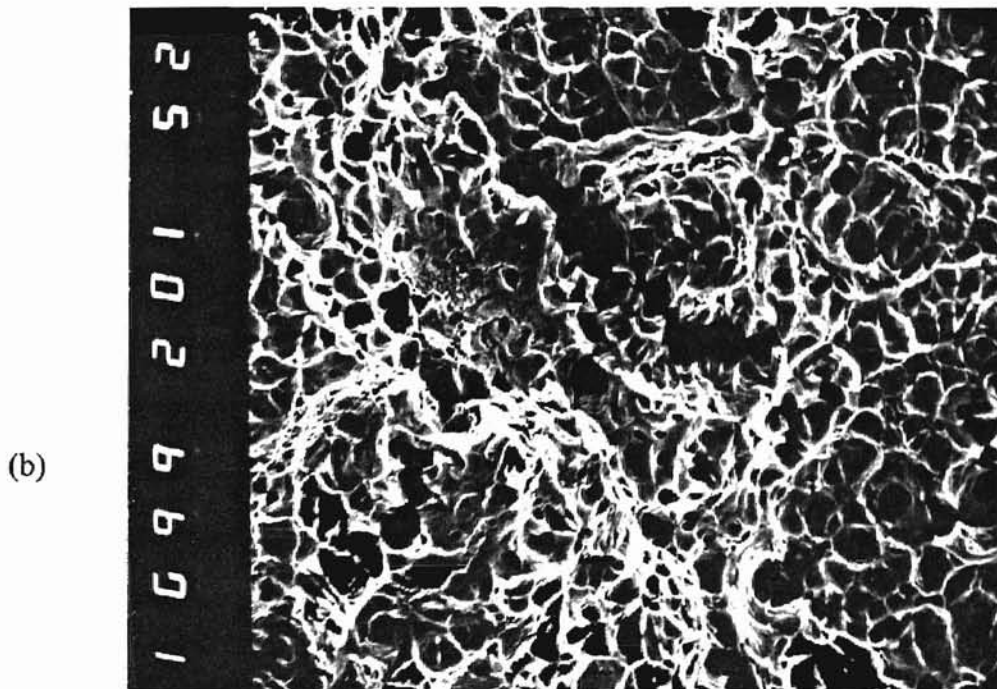
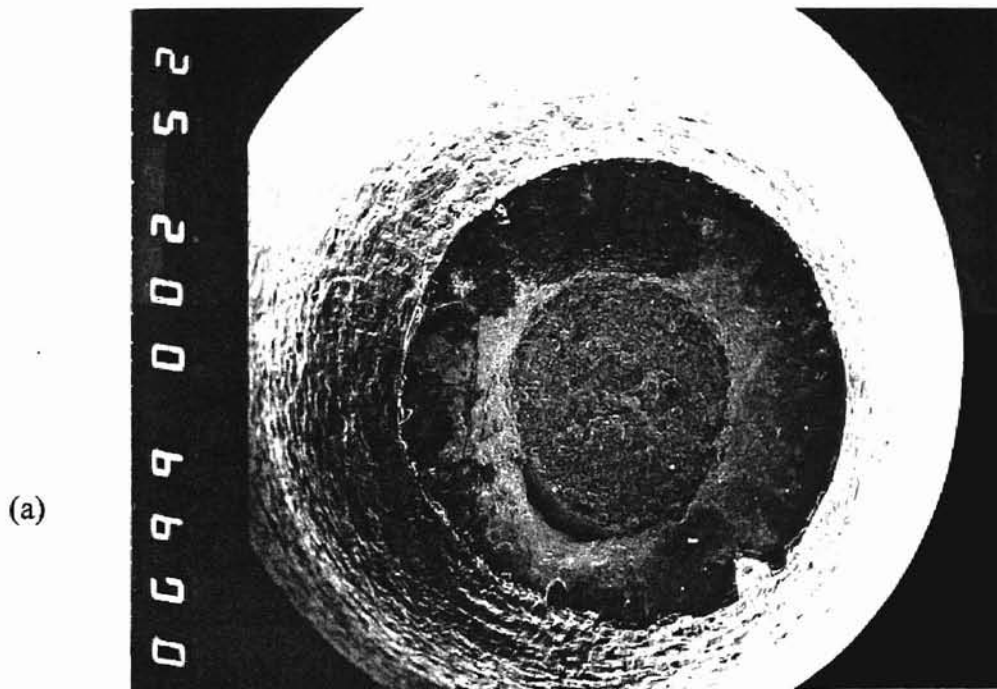


Figure 27. As-received specimen broken in air. (a) General specimen view, 20 \times . (b) Detail, showing microvoids as well as secondary MVC cracking, 1000 \times .

bands were separated, and many secondary cracks were evident. Figure 28 shows this specimen's fracture surface features. Note in Figure 28 (a) the contrast with the fracture surface of Figure 27 and the extensive secondary cracking. The region of MVC at the lower left was presumably the last zone to fracture. Therefore, the fracture origin was at top right, as viewed. Note that secondary cracking is less prominent near the origin. Note that the secondary cracking of Figure 28 (b) is apparently both IG and TG. Also, note that the grain at top right shows slip bands on three systems but no secondary cracking. Presumably, this grain fractured late, as the lack of secondary cracking indicates that the mercury-wetted crack surface was not strained significantly at this grain. The irregularity of cracking is likely a matter of irregularity of localized strain. Where strain occurs, cracking occurs. Note that the secondary cracking is not straight, implying that considerable grain strain occurred after the cracking. The annealed specimen tested in mercury was also predominately TG, but with some IG cracking present. Much secondary cracking was evident. Figure 29 shows this fracture surface. Note that this specimen is apparently more embrittled than the specimen of Figure 28; the final MVC zone at the top of Figure 29 (a) is less extensive than that of Figure 28 (a), lower left. In Figure 29 (c), note that there is less strain in the IG zone, as evidenced by the tighter secondary cracks. This photo is from just below the center of Figure 29 (b), which is in turn from the lower region of Figure 29 (a), which is opposite the MVC (final) fracture zone, and hence is in the area of fracture origin. Additionally, note the extensive slip visible on the IG fracture surfaces. In Figure 29 (d), note the noticeable slip on three systems on the IG fracture grain surfaces. Figure 29 (e) shows a detail of the TG region. Note the extensive TG secondary cracking and gaping IG secondary cracking. Figure 29 (f) is a side view of the interface between the fracture surface and the side of the specimen. Note large plastic deformation, and the secondary cracking in the z direction visible on the fracture surface. In Figure 29 (g), a detail of the side view of the fracture surface, note the elongated grains, prominent secondary cracking, and slip. Figure 29 (h) is a detail of the side of the

specimen, near the fracture surface. Figure 29 (i) is a detail of the side 6-8 mm away from the fracture, showing a side crack, and Figure 29 (j) is an intermediate location. Note the progression from longitudinal to lateral secondary crack orientation with increasing distance from the fracture surface. The waisted gage length facilitates this effect; away from the gage length center, the diameter is larger and the strain experienced is less. Additionally, while side cracking such as that seen in Figure 29 (i) and (j) was most prominent in this particular specimen, it was present in all broken specimens. Even the sensitized specimen showed small side cracks when viewed in the SZM.

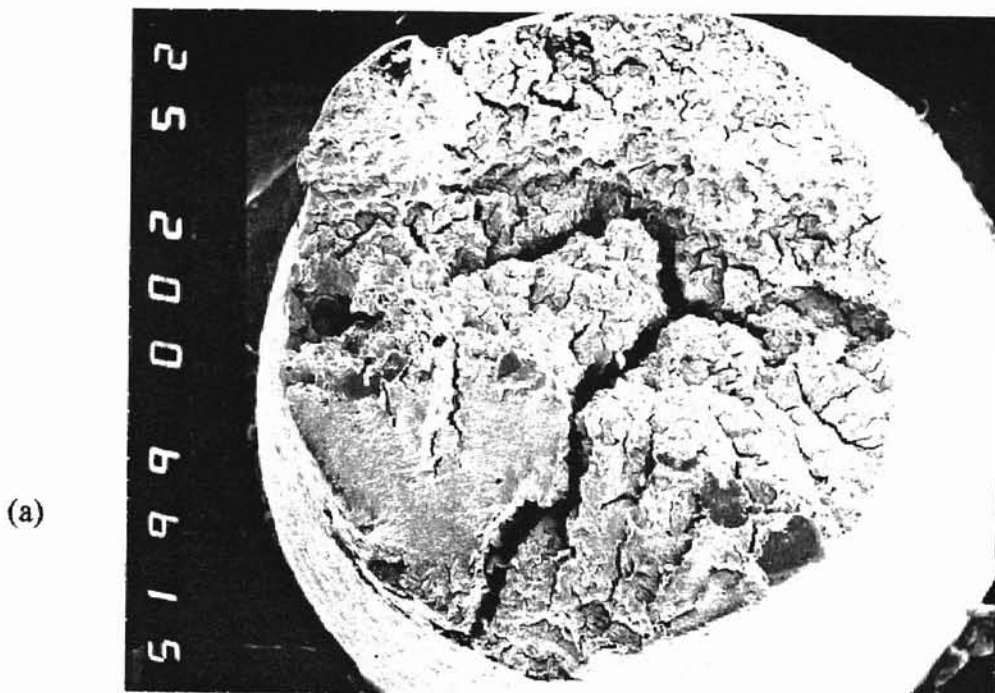
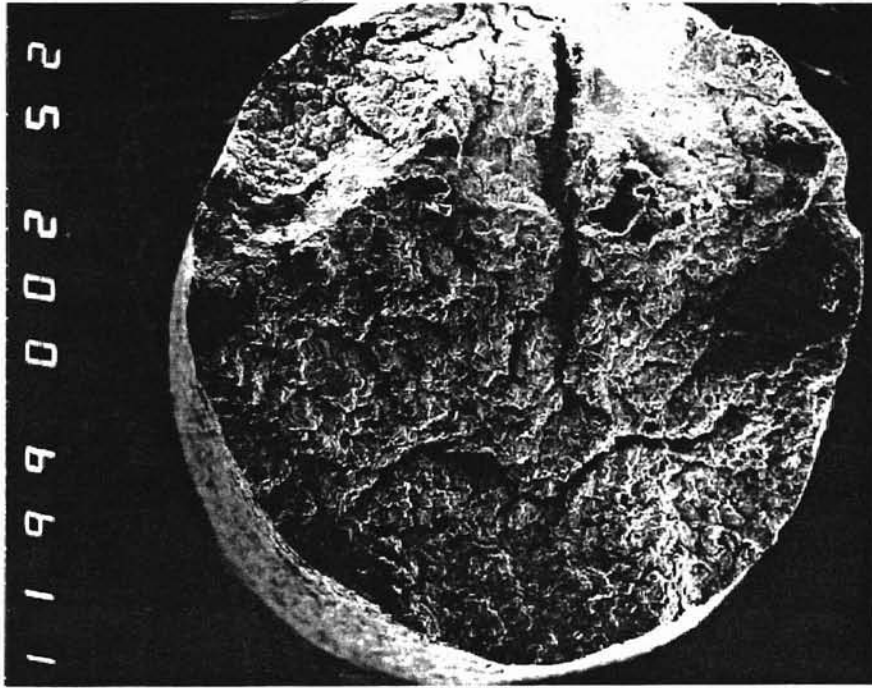


Figure 28. As-received specimen broken in mercury. (a) General specimen view, $20\times$. Note MVC smooth region, lower left. (b) Detail, $1000\times$. Note cleaved slip bands as well as some prominent slip bands on the sheared grain at the upper right.

(a)



(b)

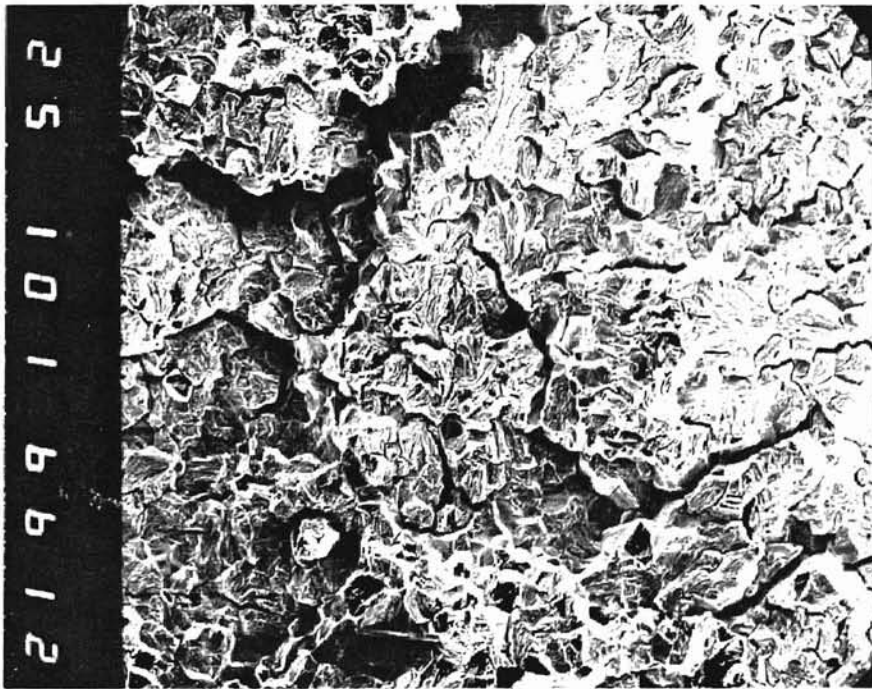


Figure 29. Annealed specimen broken in mercury. (a) General view, 20 \times . (b) Detail,

100 \times .

(c)



(d)



Figure 29, continued. (c) Detail, showing TG + IG mixed-mode cracking, $500\times$. This particular zone has an unusually high amount of IG contribution. (d) Detail of (c), $1500\times$. IG region; note slip on three systems, secondary cracking.

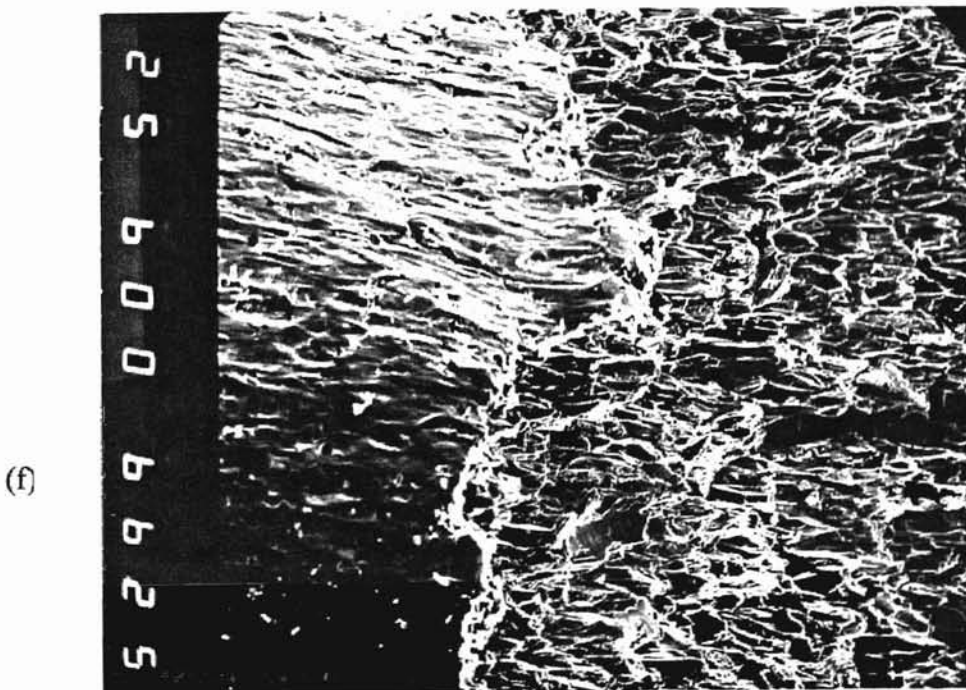
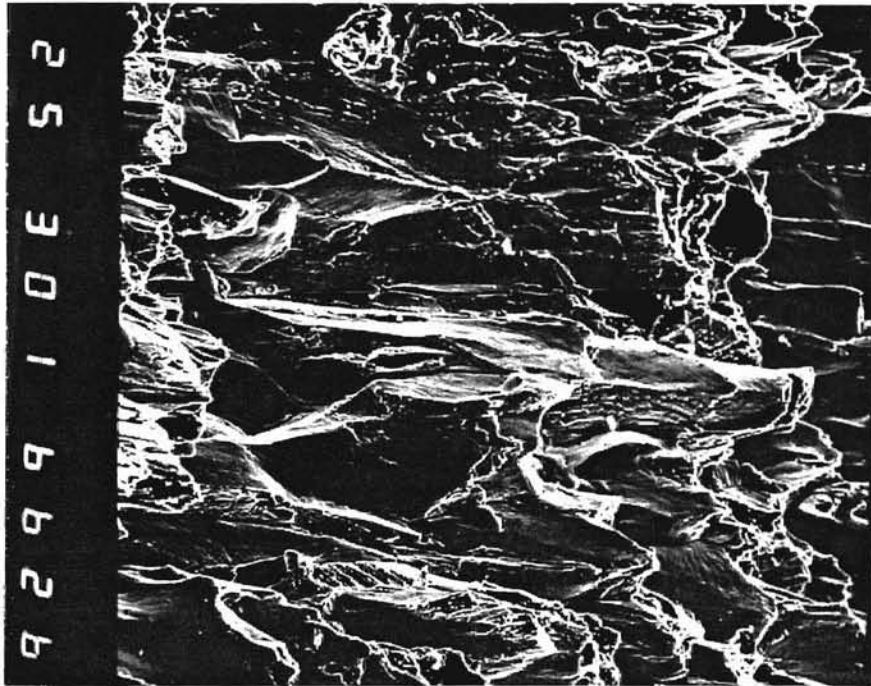


Figure 29, continued. (e) Detail of TG region of Figure 29 (c), 1500 \times . (f) Side view of fracture surface/specimen side interface, 60 \times .

(g)



(h)

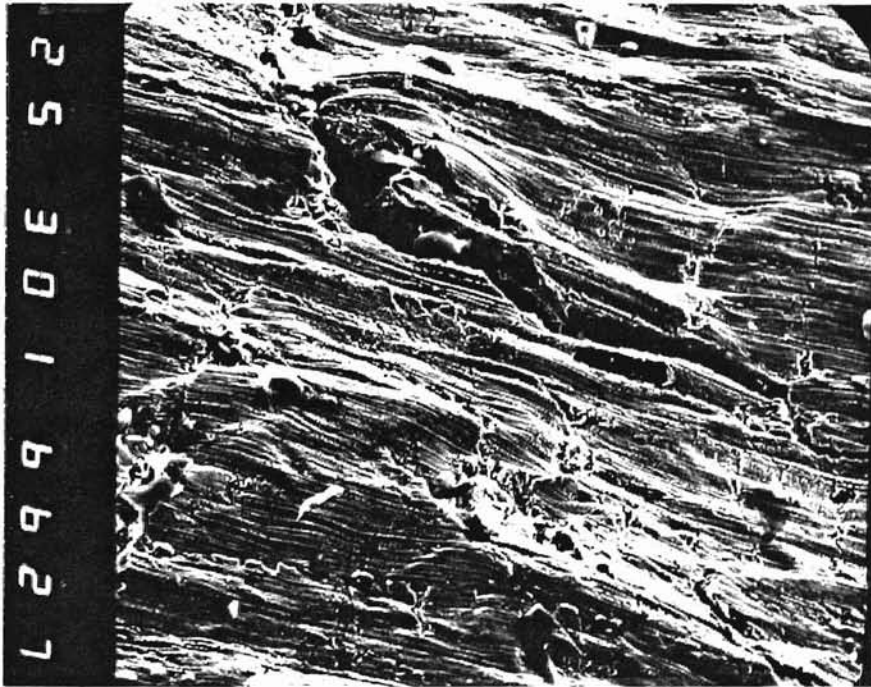
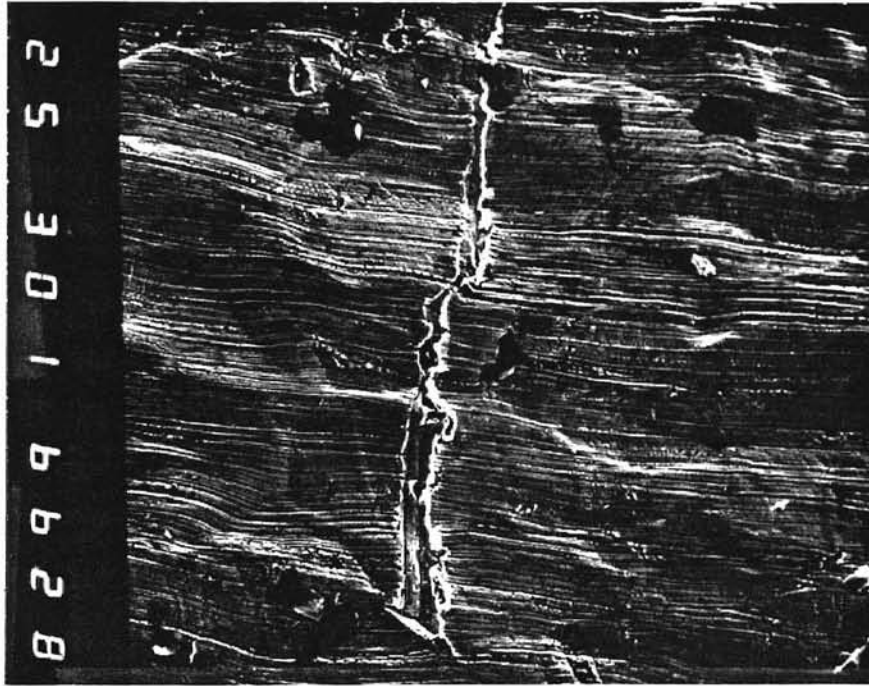


Figure 29, continued. (g) Side view of fracture surface, 300 \times . (h) Side of specimen near fracture, 300 \times .

(i)



(j)

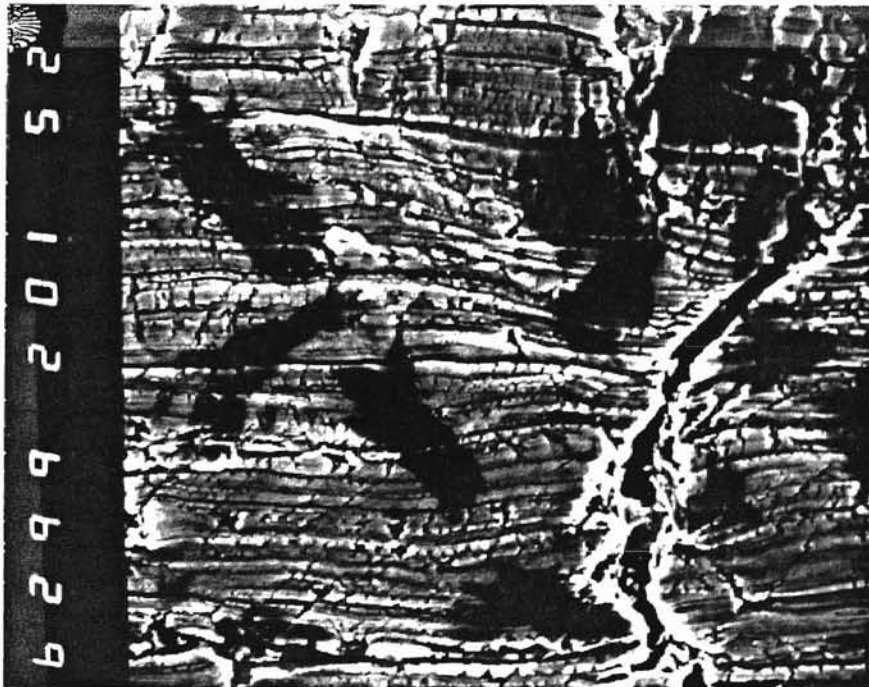


Figure 29, continued. (i) Side, 6-8 mm from fracture, $300\times$. (j) Side, between Figure 29 (h) and (i), $1000\times$.

STRAIN RATE

Published results indicate that Type 304 is strain-rate sensitive in a liquid mercury environment [15]. Additionally, an as-received specimen was broken at an extremely high strain rate (the machine's ram jumped), and the resulting fracture was barely embrittled, if at all, by the mercury. When sensitized, however, this material did not show any change in fracture behavior with strain rate. Table III details these results.

Table III. Embrittlement vs. Strain Rate

condition	strain rate (s ⁻¹)	grain size (μm)	hardness (HRB)	σ_{Fmax} (ksi)	red. of area (%)	
as rec., Hg	8.3×10^{-3}	--	--	257	63	[15]
as rec., Hg	3.3×10^{-3}	--	--	202	44	[15]
as rec., Hg	1.0×10^{-4}	--	--	181	40	[15]
as rec., Hg	5.0×10^{-6}	--	--	158	39	[15]
as rec., Hg	5.0×10^{-7}	--	--	170	38	[15]
as rec., Hg	high ($\approx 10^1$)	100-150	98	--	65	
sens., Hg	3.0×10^{-5}	100-150	81	103	34	
sens., Hg	3.0×10^{-4}	100-150	82	98	31	
sens., Hg	3.0×10^{-3}	100-150	84	94	31	

As detailed above, the fracture characteristics of Type 304 in liquid mercury are basically rate insensitive at all but relatively high strain rates. In unsensitized specimens, embrittlement was slightly more severe with increasingly slower strain rates [15]. SEM examination revealed that these specimens fractured primarily transgranularly with some intergranular contribution, with an increasingly large region of MVC as strain rates rose [15]. Figure 30 shows this progression. The as-received specimen broken at the high strain rate exhibited virtually no embrittlement in terms of reduction of area, and was not examined in the SEM. With the presence of necking as well as the high reduction of area, and the cup/cone fracture, the fracture would be largely, if not completely, MVC.

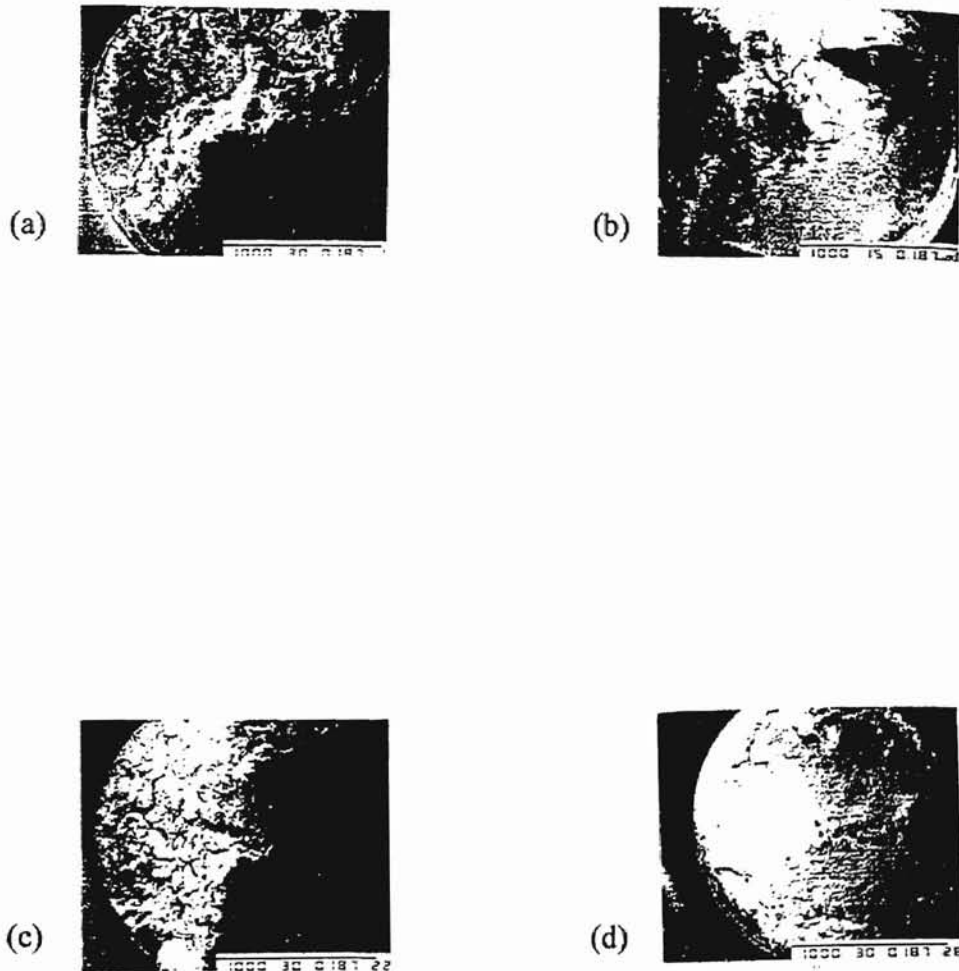


Figure 30. Fracture surfaces at various strain rates. (a) $5.0 \times 10^{-7} \text{ s}^{-1}$,
(b) $1.0 \times 10^{-4} \text{ s}^{-1}$, (c) $3.3 \times 10^{-3} \text{ s}^{-1}$, (d) $8.3 \times 10^{-3} \text{ s}^{-1}$ [15].

The sensitized specimens all had flat, intergranular fracture surfaces. Figure 31 shows a typical fracture surface of this nature. Note that slip bands are visible on the individual grains and that the secondary IG cracks often gape.

SENSITIZATION

Like nickel-base Alloy 600, Type 304 stainless is much more embrittled in the sensitized state. Fracture is completely intergranular, with no conspicuous necking. As noted above, strain rate did not affect degree of embrittlement in sensitized specimens within the range of strain rates tested. Additionally, a sensitized specimen with a much smaller grain size also exhibited the same reduction of area, although the mode of fracture was different. Table IV displays these results:

Table IV. Embrittlement vs. Sensitization

condition	strain rate (s ⁻¹)	grain size (μm)	hardness (HRB)	σ_{Fmax} (ksi)	red. of area (%)
annealed, Hg	3.0×10^{-5}	100-150	82	114	43
sens., Hg	3.0×10^{-5}	100-150	81	103	34
sens., Hg	3.0×10^{-4}	100-150	82	98	31
sens., Hg	3.0×10^{-3}	100-150	84	94	31
sens., Hg	3.0×10^{-5}	25-35	99	122	32

As mentioned above, the sensitized specimens fractured completely intergranularly, with the exception of the 25-35 μm grain size specimen, whose fracture was largely transgranular, with some microvoid coalescence in the final stages of fracture. Figures 31 and 32 show these fracture surfaces.

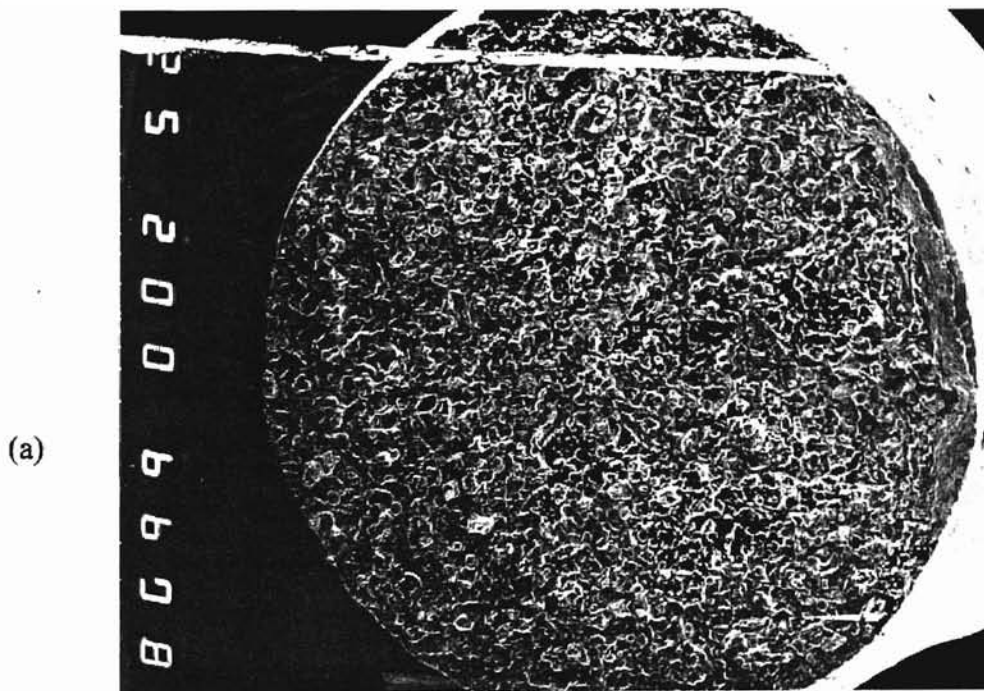


Figure 31. Fracture surface of sensitized specimen broken in mercury. (a) General specimen view, 20 \times . (b) Detail, 200 \times .

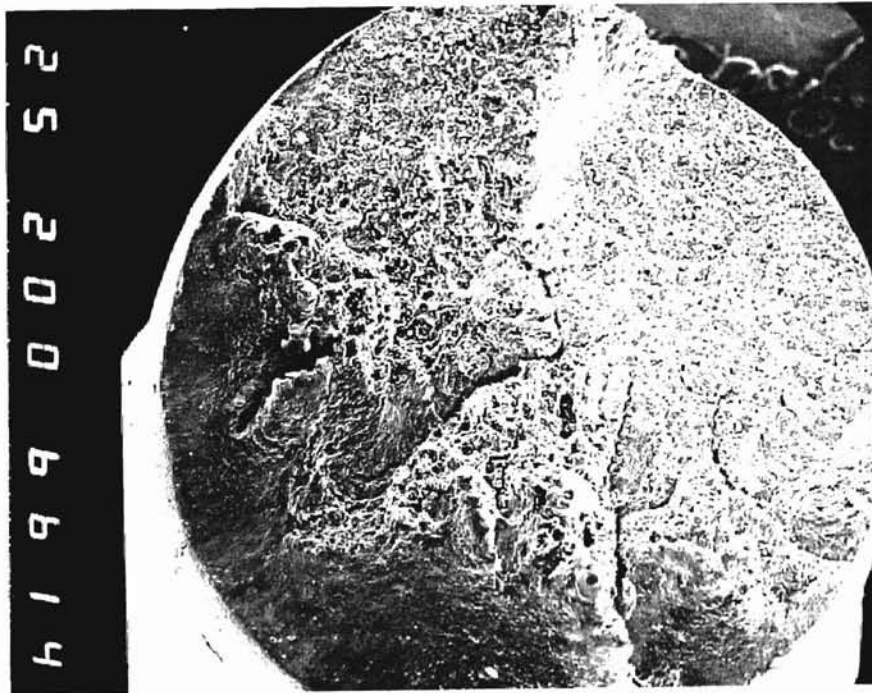


Figure 32. Sensitized small-grained specimen broken in mercury, 20 \times . Note MVC region at lower left. The origin is likely at upper right; note secondary cracking is much more conspicuous as the crack progresses.

GRAIN SIZE

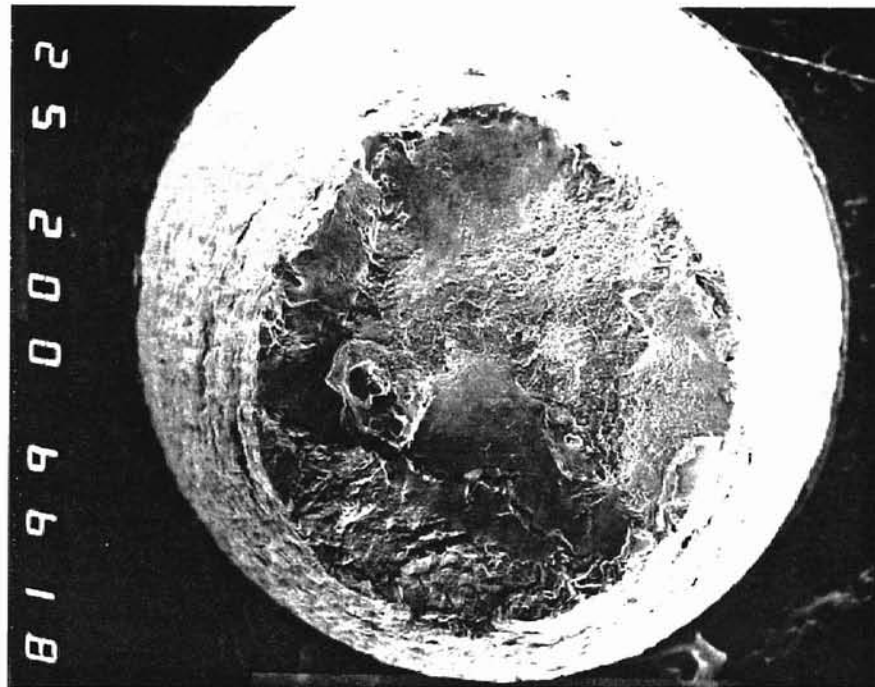
Annealed specimens with increased grain size exhibited no appreciable embrittlement. Additionally, an as-received specimen with a 25-35 μm grain size was broken in mercury; much less reduction of area occurred than with the larger-grained as-received condition from the first batch of rod. The results of these tests are presented in Table V.

Table V. Embrittlement vs. Grain Size

condition	strain rate (s^{-1})	grain size (μm)	hardness (HRB)	σ_{Fmax} (ksi)	red. of area (%)
annealed, Hg	3.0×10^{-5}	100-150	82	114	43
annealed, Hg	3.0×10^{-5}	200-350	81	112	76
annealed, Hg	3.0×10^{-5}	250-400	84	113	75
annealed, Hg	3.0×10^{-5}	300-500	84	99	69
as rec., Hg	3.0×10^{-5}	100-150	98	132	40
as rec., Hg	3.0×10^{-5}	25-35	27 HRC	171	59

In the large-grained specimens, fracture was primarily MVC, with some heavy TG shear present (almost MVC, with lots of secondary cracking). In the small-grained as-received specimen, fracture was primarily MVC with isolated pockets of TG cracking. It is unclear, however, if this fracture behavior is simply due to the small grain size, as the hardness of this specimen suggests a high degree of cold work in the as-received condition. However, the degree of cold work is certainly not as great as the amount imparted to cold-worked annealed specimens discussed in the following section, as reduction of area figures are much lower. This suggests that grain size is definitely responsible to some degree for this rod's as-received behavior. Figure 33 shows typical examples of these fractures.

(a)



(b)

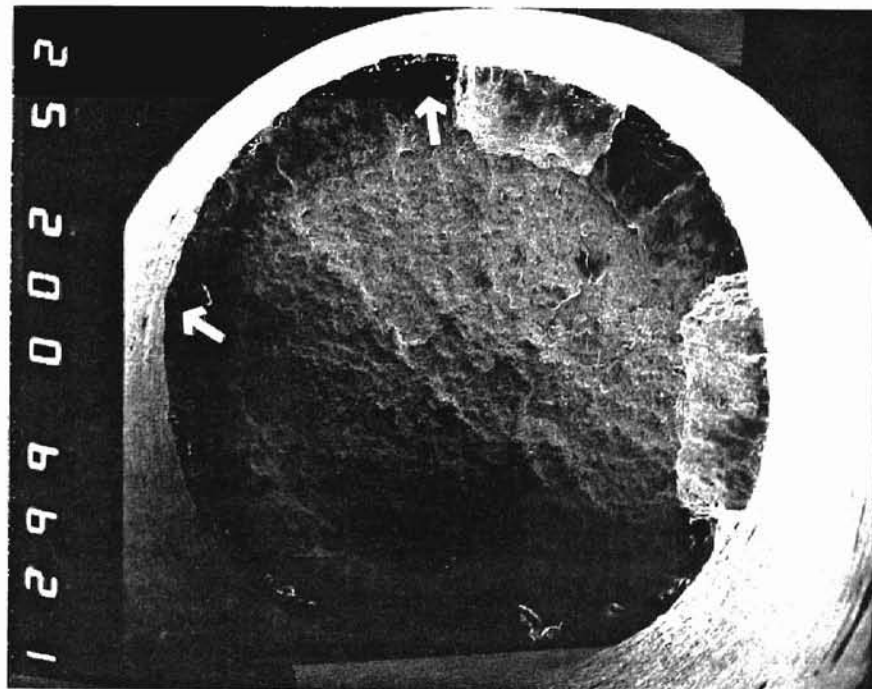


Figure 33. (a) 250-400 μm grain size specimen, broken in mercury, 20 \times . Note TG region at lower portion of fracture. (b) 25-35 μm grain size specimen, broken in mercury, 20 \times . Isolated small TG patches were found at 9 and 12 o'clock.

PRIOR COLD WORK

Specimens with prior cold work demonstrated no appreciable embrittlement.

Testing results are given in table VI.

Table VI. Embrittlement vs. Prior Cold Work

condition	strain rate (s ⁻¹)	grain size (μm)	hardness (HRB)	$\sigma_{F\text{max}}$ (ksi)	red. of area (%)
annealed, Hg ann., 70%TS	3.0×10^{-5}	100-150	82	114	43
pcw, Hg ann., 90%TS	3.0×10^{-5}	100-150	84	123	75
pcw, Hg	3.0×10^{-5}	100-150	81	129	71

Specimens with prior cold work fractured primarily by MVC, with TG cracking at the fracture origin. This TG region was similar to that seen in the large-grained specimen of Figure 33, in that there was much distortion and the appearance suggested that MVC was nearly occurring. Figure 34 shows this fracture.

FATIGUE

When tested in fatigue at 70 % of the tensile strength, fatigue life was reduced markedly in a liquid mercury environment. These results are presented in Table VII.

Table VII. Embrittlement vs. Fatigue

condition	grain size (μm)	hardness (HRB)	$\sigma_{F\text{max}}$ (ksi)	$\sigma_{F\text{min}}$ (ksi)	cycles
annealed, air	100-150	80	54	7	>1000000
annealed, Hg	100-150	80	57	7	144780

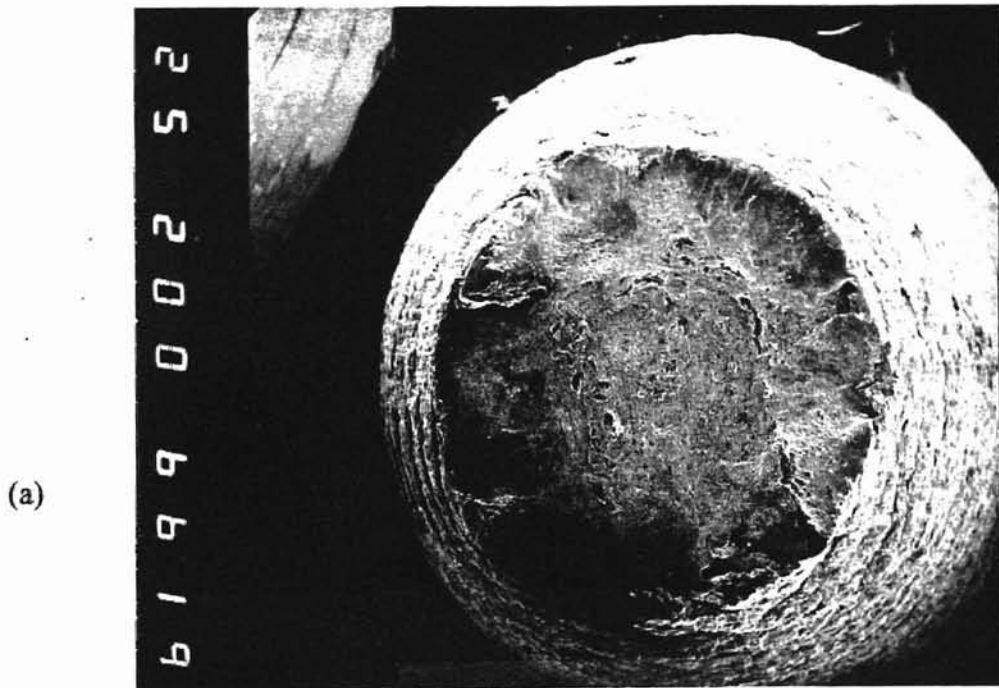


Figure 34. Fracture surface of annealed and cold-worked (to 70% of the tensile strength) specimen. (a) General view, 20 \times . (b) Detail, from 12 o'clock, showing TG origin zone and transition to MVC, 500 \times .

The fracture surface of the specimen fatigued in mercury was markedly different from the MVC that normally occurs in air [23]. The origin zone was mixed IG and TG, with a progression towards a greater proportion of TG contribution as the fracture progressed. At the end of the fatigue zone, cracking was totally TG with much plastic deformation. The overload zone was purely MVC. Figure 35 shows this fracture surface. The origin is at the lower edge of the specimen, as viewed in Figure 35 (a). Note that obvious secondary cracking is only evident in the transition to the overload zone.

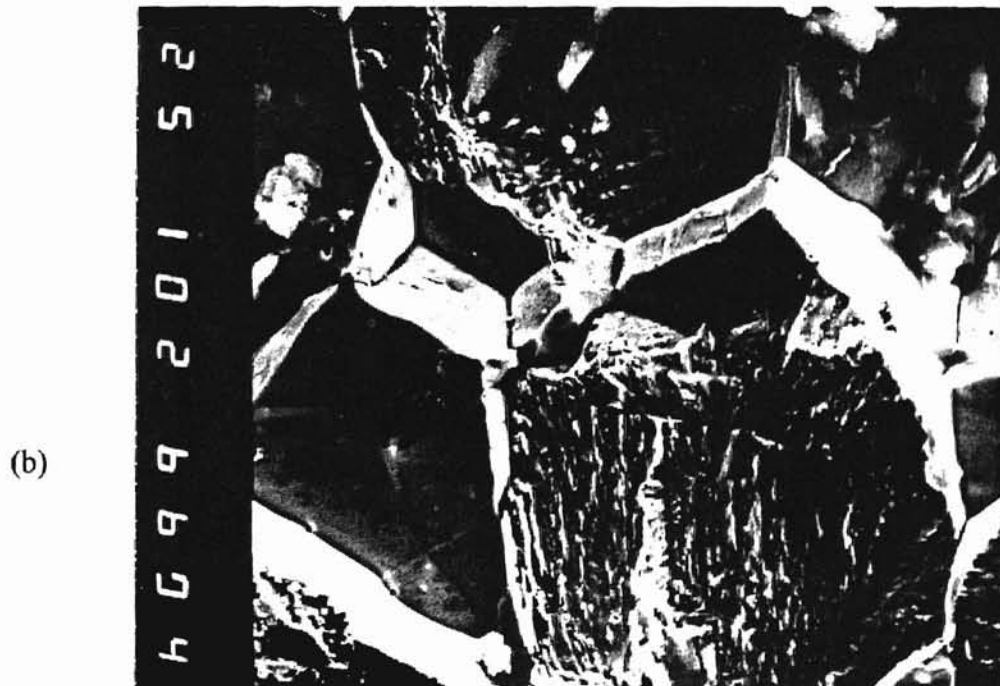
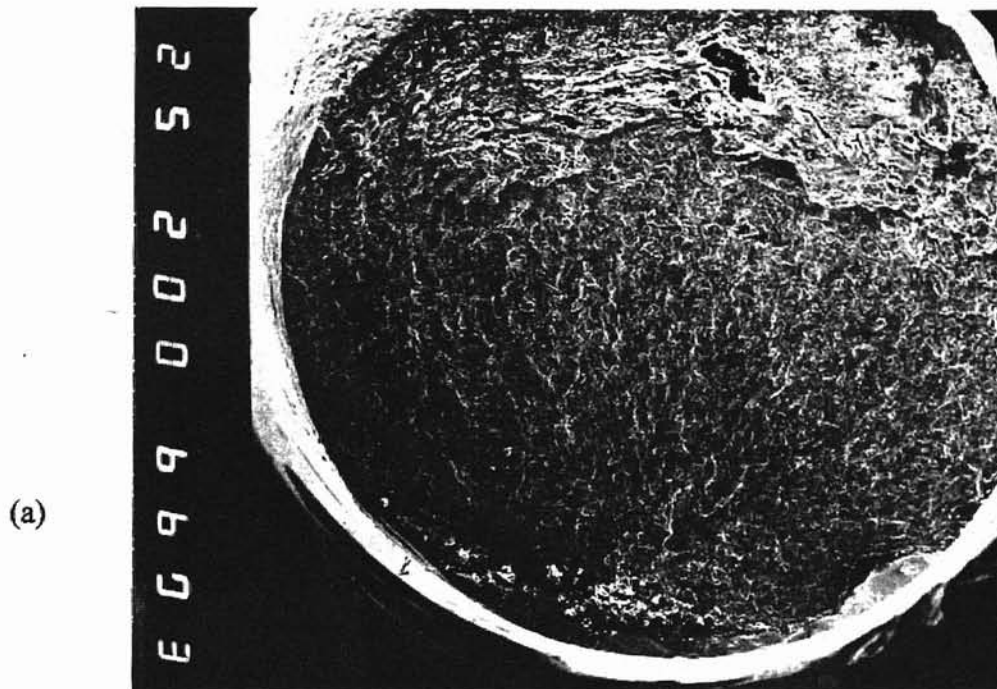


Figure 35. Annealed specimen broken in fatigue in liquid mercury. (a) General specimen view, 20 \times . (b) Mixed-mode origin, 1000 \times .

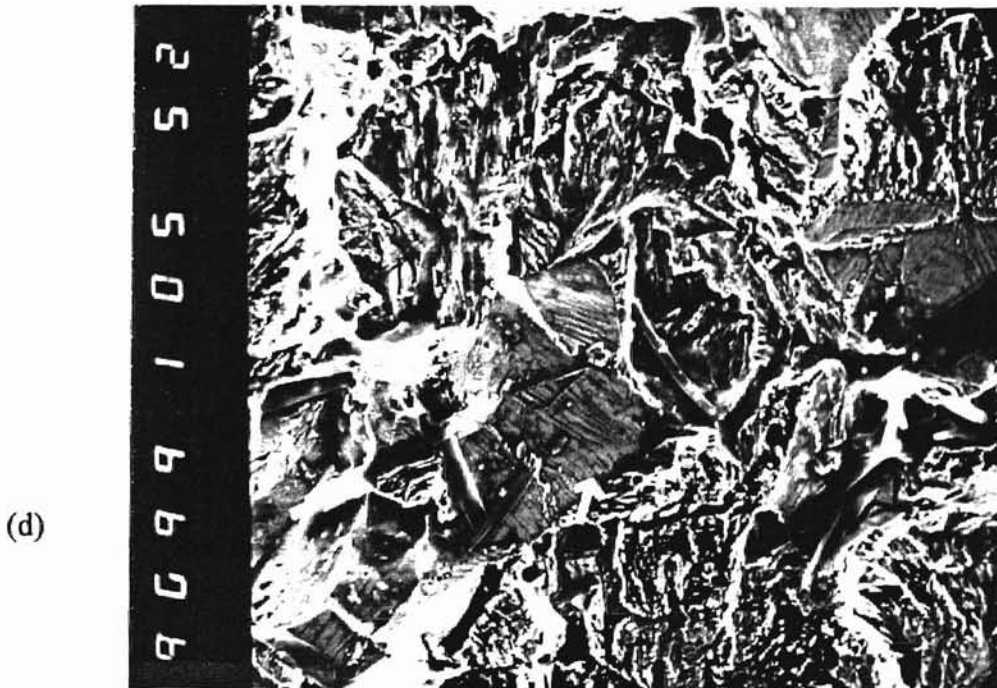
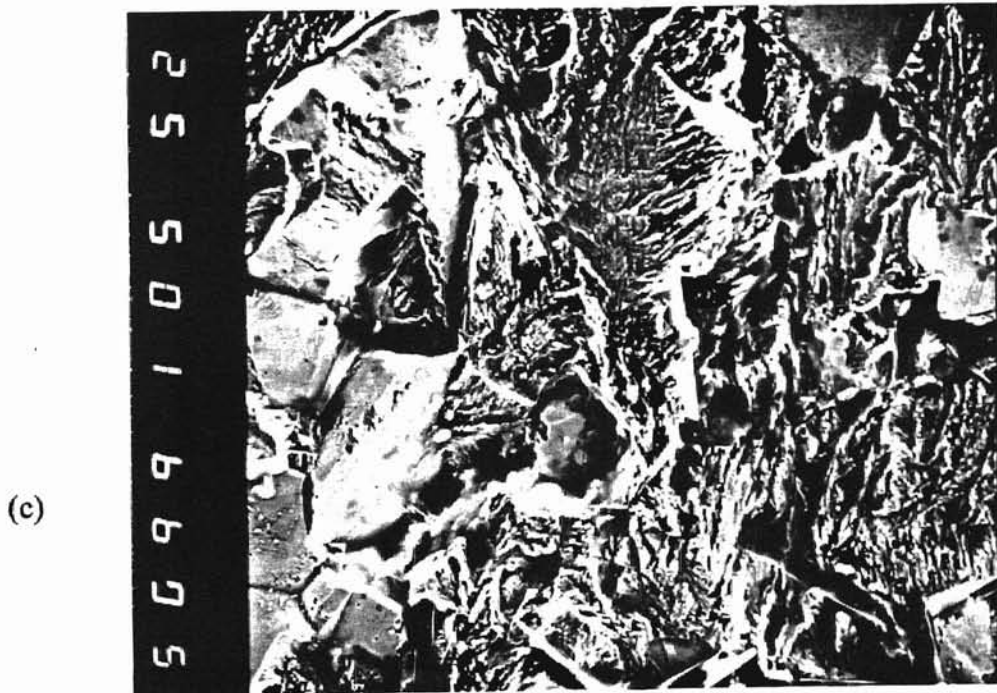


Figure 35, continued. (c) More advanced stage of fatigue crack, 500 \times . Note larger TG contribution. (d) Later stage of crack, 500 \times . Note more plastic deformation, TG cleavage, yet some IG. Note possible remains of striations, as indicated by arrow.

(e)



Figure 35, continued. (e) End of fatigue crack, 500 \times . Note large extent of PD and secondary cracking.

CHAPTER 6

DISCUSSION

WETTING BEHAVIOR

Wetting of the substrate by the liquid metal is one of the prerequisites for embrittlement. As in the nickel base alloys, it has been observed that liquid mercury does not wet unstressed stainless steel. Additionally, cleansing of mercury from fracture surfaces is possible; while the mercury can be quite stubborn in its adherence to such surfaces, this is apparently due to the droplets being mechanically wedged in crevices or nooks on the fracture surface. This argument is supported by the observation of spherical drops of mercury on the fracture surface itself; refer to Figure 24. Therefore, the conclusion is that stress/strain induced wetting is occurring at high-energy sites such as grain boundaries or slip bands.

COMPARISON WITH NICKEL BASE ALLOY EMBRITTLEMENT BEHAVIOR

Results of this study of Type 304 stainless steel's embrittlement behavior in liquid mercury are consistent with trends established by the earlier study of the nickel base alloys. Similar trends are followed for behavior with respect to grain size, prior cold work, strain rate, fractography, fatigue, and sensitization. In both nickel base alloys and Type 304 stainless, it is evident that embrittlement is most severe at an intermediate grain size. Embrittlement is limited at small grain sizes by the lack of sufficiently large dislocation pile-ups, and hence stress concentrations, at the grain boundaries. Embrittlement is limited at larger grain sizes due to ready plastic deformation, which outweighs any embrittlement phenomenon. In these two alloy systems, prior cold work acts to limit embrittlement as well as shift the fracture to a more ductile mode. In Alloy

400, the transition is from intergranular to transgranular with increasing prior cold work, while in Type 304, the transition is from transgranular to microvoid coalescence. As material is cold worked, grain boundary energy level is reduced relative to that of the interior of the grain, so it can be concluded that the reduced embrittlement is at least partly due to a reduction in wetting at the grain boundaries. While cold work also makes an intergranular fracture path more difficult, it is unlikely that this phenomenon is responsible for decreased embrittlement in the case of Type 304, as fracture of annealed material was already mostly transgranular. A similar trend is seen with varying strain rate. Embrittlement is more severe at lower strain rates; at higher strain rates a transition of fracture mode to MVC is observed. Presumably, wetting is not occurring until a certain stress level is reached; failure then comes soon thereafter. Both nickel base alloys and Type 304 stainless exhibit similar fractographies with respect to strain at failure. The most embrittled examples have a low strain to failure, with an intergranular fracture mode present. Less embrittled examples show more plastic deformation on the fracture surface, with a transition from transgranular cracking to microvoid coalescence occurring with increasing strain at fracture. Additionally, there is typically a progression across the fracture surface, from more embrittlement to less. That is to say, the origin zone will likely be intergranular or transgranular, while final stages of fracture are often TG or microvoid coalescence. This effect is presumably due to increased strain having occurred by the time the crack has propagated across the specimen. Both nickel-base alloys and Type 304 are more embrittled in fatigue testing, with fracture by a more brittle mode than in tensile testing, except in the case of Alloy 400, whose fracture in tensile testing is completely intergranular. Fracture in fatigue of Alloy 400 is also completely IG. Alloys 200, 600, and 800 show a transition from predominately MVC with some TG (800 was not embrittled in tensile testing in mercury) to IG/TG in fatigue [16]. Similarly, Type 304 shows a transition from TG, tensile, to IG, fatigue. This is to be expected, as fatigue testing represents the most severe testing condition, for both air and mercury

environments. In fatigue, of course, failure occurs below the tensile strength of the material. In an embrittling environment, it stands to reason that the fatigue crack, once initiated (which is likely facilitated by the embrittler species), will be subject to embrittlement through its entire slow propagation, which occurs without the significant strain responsible for less embrittlement occurring as a propagation-controlled crack propagates in a slow-strain-rate test. Finally, sensitization greatly increases embrittlement; in both Alloy 600 and Type 304 there is a transition to fully intergranular fracture when tested in the sensitized state.

SIMILARITY TO 800 SERIES NICKEL BASE ALLOY BEHAVIOR

As expected, there are a number of similarities of embrittlement behavior between the similarly-composed 800 series of nickel-base alloys and Type 304 stainless steel. The 800 series are not embrittled in slow strain rate testing; however, the preponderance of 45 degree side cracks near the fracture indicates that embrittlement is very close to occurring. Type 304, while embrittled, is not embrittled to a significant degree, as, for example, Alloy 400 is. In the nickel base alloys it was noted that embrittlement was lessened with increasing iron content. The 800 series are embrittled in fatigue, however, and correspondingly, an increase in embrittlement of Type 304 occurs in fatigue testing.

SIMILARITY TO ALLOY 600 WITH RESPECT TO SENSITIZATION

Like Alloy 600, Type 304 is much more embrittled by mercury when sensitized. Fracture is completely intergranular. Presumably the grain boundary precipitate resulting from sensitization heat treatment allows crack initiation and propagation to occur at much lower strain levels than when the material is unsensitized. The fact that no change of reduction of area occurs in the small-grained sensitized specimen indicates that crack

initiation is occurring at the same stress level, and hence amount of strain, as in larger-grained specimens, despite the shift in fracture morphology.

NUCLEATION VERSUS PROPAGATION CONTROL

In Type 304, embrittlement is entirely by the propagation control mechanism. In all specimens, conspicuous side cracking indicates propagation control. Even the all-intergranular fracture, sensitized specimens, small side cracks were visible, even under the SZM. The presence of visible plastic deformation in the grains of these fracture surfaces, as well as the gaping secondary cracking, indicates that embrittlement is propagation-controlled. These intergranular secondary cracks presumably open up while the still-wetted surface is strained by nearby plastic deformation processes. Apparently, the uniformly intergranular nature of these fracture surfaces is a product of the sensitization encouraging intergranular cracking and is not evidence for the occurrence of nucleation control. Additionally, reduction of area figures are too high for nucleation control; nucleation-controlled embrittlement would result in RAs of $< 5\%$. In propagation-controlled cracking, the issue of what is causing this mode of fracture control to occur must be addressed. The most likely possibility is that plastic deformation at the crack tip, and consequent crack blunting, is actually facilitated by the presence of liquid mercury. Such would be the case if the embrittler species were responsible for the reduction of shear strength of atomic bonds at the crack tip, as suggested by one of the proposed embrittlement mechanisms [6]. Additionally, macroscopic plastic deformation of the material facilitated by the propagation control also would be responsible for crack tip blunting. Apparently the crack can continue propagating when increasing load levels cause a sufficient stress concentration to rematerialize. In propagation control, the first crack usually does not lead to failure, with several cracks arrested before stresses are sufficiently high to propagate one to failure. Specimens with multiple side cracks suggest

that this may be occurring, with many cracks arrested, and one (or several convergent) eventually propagating to failure when the applied stress level is sufficiently high.

CHAPTER 7
SUMMARY OF RESULTS

The results of this study are as follows:

- 1) Type 304 stainless is not wetted by mercury in the unstressed state; wetting is stress-induced at high-energy sites.
- 2) Embrittlement by liquid mercury is more severe at lower strain rates.
- 3) As in the case of nickel-base Alloy 600, sensitized material is much more embrittled, and sensitization seems to remove grain size dependence as well as some degree of strain rate dependence of embrittlement severity.
- 4) Severity of embrittlement is maximum at an intermediate grain size.
- 5) Prior cold work inhibits embrittlement.
- 6) Embrittlement is more severe in fatigue loading.
- 7) There is correlation of embrittlement trends with the behavior of the nickel-base 800 series of alloys.

CHAPTER 8

SUGGESTIONS FOR FURTHER RESEARCH

The following are suggestions for further research on the liquid metal embrittlement of AISI Type 304 stainless steel:

- 1) Examination of a greater variation of grain sizes to pinpoint that at which embrittlement is maximum.
- 2) Testing of sensitized material with prior cold work.
- 3) Testing of sensitized material in fatigue.
- 4) Experimentation at a range of temperatures to determine whether an embrittlement trough exists, and if so, at what temperature embrittlement is maximum in this system.

BIBLIOGRAPHY

1. P. J. L. Fernandes, R. E. Clegg, and D. R. H. Jones, "Failure by Liquid Metal Induced Embrittlement," *Engineering Failure Analysis* **1**, 1 (1994) pp. 51-63
2. M. H. Kamdar, "Liquid Metal Embrittlement," *Treatise on Materials Science and Technology* **25** (1983) pp. 361-459
3. D. A. Wheeler, R. G. Hoagland, and J. P. Hirth, "Evidence for Crack Tip Oxidation Effects During the Liquid Metal Embrittlement of AA 7075 Aluminum Alloy by Liquid Mercury," *Corrosion* **45**, 3 (1989) pp. 207-212
4. P. Skeldon, J. P. Hilditch, J. R. Hurley, and D. R. Tice, "The Liquid Metal Embrittlement of 9Cr Steel in Sodium Environments and the Role of Non-metallic Impurities," *Corrosion Science*, **36**, 4 (1994) pp. 593-610
5. N. S. Stoloff, "Recent Developments in Liquid-Metal Embrittlement," *Environment-Sensitive Fracture of Engineering Materials* (Edited by Z. A. Foroulis), AIME, Warrendale, PA (1979) pp. 486-518
6. M. H. Kamdar, *Liquid Metal Embrittlement*, ASM Metals Handbook, 9th Edition **11** (1987) pp. 225-244
7. C. E. Price and R. K. King, "The Embrittlement of Monel 400 By Hydrogen and Mercury, as a Function of Temperature," *Corrosion Cracking* (Edited by V. S. Goel), Conference Proceedings, 81-88, ASM, Metals Park, OH (1986)
8. L. P. Costas, "Effect of Phosphorus on the Embrittlement of Copper-Nickel Alloys by Mercury," *Corrosion-NACE*, **31**, 3 (1975) pp. 91-96
9. C. E. Price, G. R. Peevy, and J. K. Willoughby, "The Effect of Prestress on the Embrittlement of Monel 400 by Mercury," *Scripta METALLURGICA*, **20**, 9 (1986) pp. 1297-1298
10. C. E. Price and R. S. Fredell, "A Comparative Study of the Embrittlement of Monel 400 at Room Temperature by Hydrogen and Mercury," *Metallurgical Transactions*, **17A**, May 1986 pp. 889-898
11. Jerry J. English and Gregory Kobrin, "Liquid Mercury Embrittlement of Aluminum," *Materials Performance*, February 1989, pp. 62-63

12. C. E. Price and J. K. Good, "The Fatigue Behavior of Nickel, Monel, and Selected Superalloys, Tested in Liquid Mercury and Air; A Comparison," *ASME Transactions*, **H**, 106 (1984) pp. 178-183
13. C. E. Price and J. K. Good, "The Fractography of Hydrogen and Mercury Embrittlement in Inconel 600," *Journal of Materials Engineering*, **9**, 3 (1987) pp. 283-291
14. C. E. Price and J. K. Good, "The Tensile Fracture Characteristics of Nickel, Monel, and Selected Superalloys Broken in Liquid Mercury," *ASME Transactions*, **H**, 106 (1984) pp. 184-190
15. J. J. Krupowicz, "Slow Strain Rate Fracture Characteristics of Steel and Aluminum Alloys Tested in Mercury Environments," *Journal of Engineering Materials and Technology*, **111**, 3 (1989) pp. 229-234
16. C. E. Price and J. A. Morris, "The Comparative Embrittlement of Example Nickel Alloys by Hydrogen and Mercury," *Journal of Materials for Energy Systems*, **7**, 3 (1985) pp. 246-255
17. A. W. Funkenbusch, L. A. Heldt, and D. F. Stein, "The Influence of Grain Boundary Phosphorus Concentration on Liquid Metal and Hydrogen Embrittlement of Monel 400," *Metallurgical Transactions A*, **13A**, April 1982 pp. 611-618
18. C. E. Price and Sheng Loong Tai, "Sensitization, Pitting, Crevice Corrosion, and Environmental Assisted Cracking in Alloy 600," *NACE Corrosion '93*, Paper No. 181
19. Kenneth G. Budinski, *Engineering Materials: Property and Selection*, 4th Edition, Prentice-Hall, Englewood Cliffs, NJ (1992) pp. 435-438
20. *U. S. Air Force Structural Alloys Handbook*, 1994 edition, Edited by C. Y. Ho, Vol. 2, p. 134.
21. *Metallographic Technique for Wrought Stainless Steels*, ASM Metals Handbook, 8th Edition, **8** (1973) pp. 97-99
22. ASTM specification A 262-91, *Standard Practices for Detecting Susceptibility to Intergranular Attack in Austenitic Stainless Steels*.

23. *IITRI Fracture Handbook: Failure Analysis of Metallic Materials by Scanning Electron Microscopy*, Edited by S. Bhattacharyya, V. E. Johnson, S. Agarwal, and M. A. H. Howes, Metals Research Division, IIT Research Institute, Chicago, IL (1979) pp. 339-349.

VITA

Timothy John Clark

Candidate for the Degree of

Master of Science

Thesis: LIQUID METAL EMBRITTLEMENT OF TYPE 304 STAINLESS
STEEL BY LIQUID MERCURY

Major Field: Mechanical Engineering

Biographical:

Education: Graduated from Deer Creek High School, Edmond, Oklahoma in May 1989; received Bachelor of Science degree in Mechanical Engineering from Oklahoma State University, Stillwater, Oklahoma in December 1993. Completed the requirements for the Master of Science degree with a major in Mechanical Engineering at Oklahoma State University in December 1995.

Experience: Employed by Oklahoma State University, Department of Mechanical and Aerospace Engineering as an undergraduate research assistant, June-December 1993, and as a graduate teaching assistant, January 1994-May 1995.

Professional Memberships: Pi Tau Sigma, American Society of Mechanical Engineers